





## PAPER

[View Article Online](#)  
[View Journal](#) | [View Issue](#)Cite this: *Dalton Trans.*, 2024, **53**, 12527

# Position of substituents directs the electron transfer properties of entatic state complexes: new insights from guanidine-quinoline copper complexes†

Joshua Heck,  Anastasia Kucenko,  Alexander Hoffmann  and Sonja Herres-Pawlis \*

In a previous study, we showed that the properties and the ability as an entatic state model of copper guanidine quinoline complexes are significantly influenced by a methyl or methyl ester substituent in the 2-position. To prove the importance of the 2-position of the substituent, two novel guanidine quinoline ligands with a methyl or methyl ester substituent in the 4-position and the corresponding copper complexes were synthesized and characterized in this study. The influence of the substituent position on the copper complexes was investigated with various experimental and theoretical methods. The molecular structures of the copper complexes were examined in the solid state by single-crystal X-ray diffraction (SCXRD) and by density functional theory (DFT) calculations indicating a strong dependency on the substituent position compared to the systems substituted in the 2-position from the previous study. Further, the significantly different influence on the donor properties in dependency on the substituent position was analyzed with natural bond orbital (NBO) calculations. By the determination of the redox potentials, the impact on the electrochemical stabilization was examined. With regard to further previously analyzed guanidine quinoline copper complexes, the electrochemical stabilization was correlated with the charge-transfer energies calculated by NBO analysis and ground state energies, revealing the substituent influence and enabling a comparatively easy and accurate possibility for the theoretical calculation of the relative redox potential. Finally, the electron transfer properties were quantified by determining the electron self-exchange rates *via* the Marcus theory and by theoretical calculation of the reorganization energies *via* Nelsen's four-point method. The results gave important insights into the dependency between the ability of the copper complexes as entatic state model and the type and position of the substituent.

Received 26th May 2024,  
Accepted 8th July 2024

DOI: 10.1039/d4dt01539h

[rsc.li/dalton](http://rsc.li/dalton)

## Introduction

Copper proteins are crucial for many processes in all living organisms. For fast and reversible electron transfer processes, type 1 copper proteins are responsible.<sup>1</sup> In the active site, they possess a copper center coordinated by four donors in a distorted coordination geometry, whereby the donors are two histidines (N donor), one cysteine (S donor) and in most cases

one methionine (S donor).<sup>2</sup> The fast electron transfer is represented by high electron self-exchange rates  $k_{11}$  ranging from  $\sim 10^3$  to  $\sim 10^6 \text{ M}^{-1} \text{ s}^{-1}$ .<sup>3</sup> This characteristic property of the type 1 copper proteins led to the introduction of the term “entatic state” by Vallee and Williams in 1968.<sup>4</sup> The entatic state principle is not limited to type 1 copper proteins but also applicable to other metalloproteins and proteins without a metal ion. According to the definition, the protein exhibits a rigid framework that does not allow, in the case of a metalloprotein, the metal ion in the active site to exist with its energetically preferred coordination geometry. The resulting energization leads to the efficiency of the protein.<sup>4,5</sup> Further possibilities for the energization of a protein were suggested and discussed in the literature.<sup>5–8</sup> The “rack” mechanism was proposed by Lumry and Eyring and it explains the energization by significant structural changes of the protein framework caused by allosteric effects and by a possibly adverse structural configuration for the metal ion.<sup>9</sup> In contrast, in the “induced fit”

Institute of Inorganic Chemistry, RWTH Aachen University, Landoltweg 1a, 52074 Aachen, Germany. E-mail: [sonja.herres-pawlis@ac.rwth-aachen.de](mailto:sonja.herres-pawlis@ac.rwth-aachen.de)

† Electronic supplementary information (ESI) available: Experimental data of the methods and details of the synthesis with characterization (NMR and IR spectroscopy and mass spectrometry), crystallographic information, UV/Vis-spectra, CVs and stopped-flow UV/Vis spectra, DFT details, NMR spectra, additional plots and further discussions. CCDC 2358203–2358207. For ESI and crystallographic data in CIF or other electronic format see DOI: <https://doi.org/10.1039/d4dt01539h>



mechanism, the protein framework possesses a local flexibility that leads to an enforced coordination geometry of the metal ion.<sup>10</sup> In the “induced-rack” theory by Malmström, the protein framework has a certain degree of flexibility resulting ideally in two different protein structures. In one structure, the protein framework is relaxed but the coordination geometry around the metal ion is strained and, therefore, energetically unfavorable. In the other structure, the coordination geometry around the metal ion is relaxed but the protein framework is strained and, therefore, energetically unfavorable.<sup>11</sup> The “electronic entatic state” was proposed by Rorabacher *et al.* As for the entatic state, the structural strain of the protein is an important factor but further, the influence of electronic effects is considered.<sup>12</sup> Comba suggested a generalized definition by naming the energization as entasis caused by adverse interactions between the metal ion and ligand sphere.<sup>6,13</sup> In any case how the energization is explained, it results in a faster reaction because the energy levels of the reactants and products are closer to the energy level of the transition state resulting in a smaller activation energy. The entatic state of type 1 copper proteins can be explained by the extraordinary coordination sphere around the copper center. Which deviates significantly from the ideal tetrahedral coordination geometry preferred by Cu(I) and the ideal square-planar coordination geometry preferred by Cu(II).<sup>6</sup> Further, the coordination sphere is very similar in the Cu(I) and the Cu(II) species. Both aspects result in a facilitated transition between the oxidation states and, therefore, an enhanced electron transfer. Parallel, the concept of the “in-between-state” has been proposed by Falcone and Hureau for intrinsically disordered peptides in copper binding proteins.<sup>14</sup>

Meanwhile, the entatic state principle is applied to explain the improved activity in catalysis or certain properties of metal complexes besides a biological background.<sup>7,15</sup> Various copper complexes were reported as model complexes for type 1 copper proteins and their electron self-exchange rates (Fig. 1). The redox couples  $[\text{Cu}(\text{bib})_2]^{+/2+}$  and  $[\text{Cu}(\text{bite})]^{+/2+}$  by Stanbury *et al.* exhibit very small electron self-exchange rates  $k_{11}$ .<sup>16</sup> Comba *et al.* reported a copper complex redox couple of a rigid bispidine ligand and its electron transfer properties.<sup>13,17</sup> Due to its inflexibility, the bispidine ligand is preorganized resulting in a low internal reorganization energy  $\lambda_i$ . Nevertheless, the metal ion is not fixed in the ligand cavity during the electron transfer resulting in a significant rearrangement of the solvent sphere and, therefore, a high solvent reorganization energy  $\lambda_s$ . In sum, this leads to a low electron self-exchange rate  $k_{11}$  of  $\sim 10^1 \text{ M}^{-1} \text{ s}^{-1}$  in water at 25 °C.<sup>17</sup> This result demonstrates that the reorganization of the ligand and solvent sphere is crucial for the electron transfer. However, also copper complex redox couples with high  $k_{11}$  values comparable with those of type 1 copper proteins are known. The redox couple  $[\text{Cu}([15]\text{aneS}_3\text{bpy})]^{+/2+}$  by Rorabacher *et al.* exhibits a  $k_{11}$  of  $\sim 10^5 \text{ M}^{-1} \text{ s}^{-1}$  in MeCN at 25 °C which is similar to the redox couple  $[\text{Cu}(\text{H}_2\text{Tpy}^{\text{NMe}_5})\text{Cl}]^{0/+}$  by Szymczak *et al.* with a  $k_{11}$  of  $\sim 10^5 \text{ M}^{-1} \text{ s}^{-1}$  in THF at room temperature.<sup>12,18</sup> For several years, we examined copper guanidine quinoline complex redox couples as

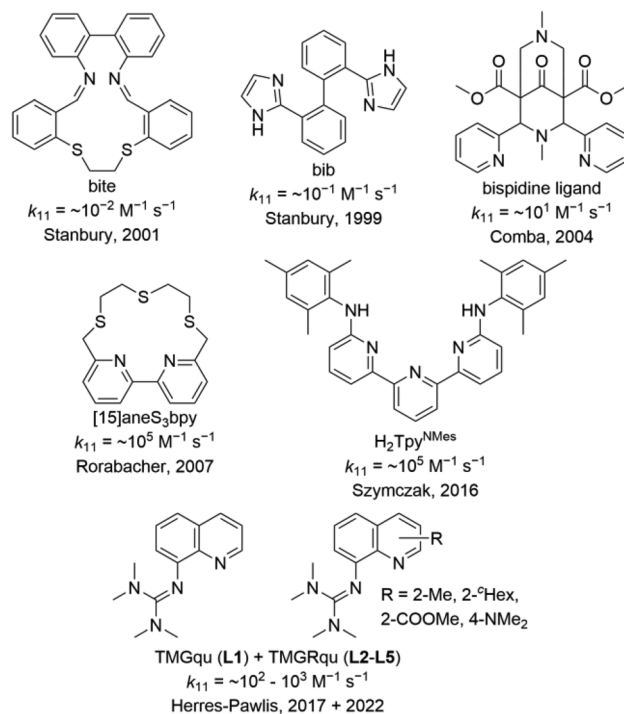


**Fig. 1** Ligands used to synthesize copper complexes that were analyzed as entatic state model complexes for the electron transfer.<sup>12,13,16–19,21,23</sup>

entatic state models. Due to the significantly distorted coordination geometries of the Cu(I) and Cu(II) species from the ideal coordination geometries, the related Cu(I) and Cu(II) species of a redox couple possess very similar structures.<sup>19–23</sup> The influence of different guanidine moieties and substitution position was examined in the electron transfer. The TMG moiety enabled higher  $k_{11}$  values compared to the DMEG moiety due to a higher similarity of the Cu(I) and Cu(II) species.<sup>21</sup> Various substituents in the 2-, 4- and 6-position were tested whereby a methyl and methyl ester substituent in the 2-position of TMG2Mequ (L2) and TMG2Meequ (L4) induced the strongest enhancement of the electron transfer properties.<sup>22,23</sup> Therefore, an increase in  $k_{11}$  by one order of magnitude from  $\sim 10^2 \text{ M}^{-1} \text{ s}^{-1}$  for  $[\text{Cu}(\text{TMGqu})_2]^{+/2+}$  (C1/C2) to  $\sim 10^3 \text{ M}^{-1} \text{ s}^{-1}$  for  $[\text{Cu}(\text{TMG2Mequ})_2]^{+/2+}$  (C3/C4) and  $[\text{Cu}(\text{TMG2Meequ})_2]^{+/2+}$  (C5/C6) in MeCN at 25 °C was observed. In the case of  $[\text{Cu}(\text{TMG2Mequ})_2]^{+/2+}$  (C3/C4), we explained the increase with the higher similarity between the Cu(I) and Cu(II) species caused by the steric demand of the methyl substituent and in the case of  $[\text{Cu}(\text{TMG2Meequ})_2]^{+/2+}$  (C5/C6), with the various influences of the methyl ester substituent on the copper complexes.<sup>23</sup>

In this study, two novel ligands with a methyl or methyl ester substituent in the 4-position were synthesized. The substituent influence on the properties of the corresponding copper complexes was examined by a plethora of experimental and theoretical methods. The results are discussed in relation to those of the previous study.



## Results and discussion

### Synthesis of the ligands

The synthesis of **L7** and **L8** proceed analogously from the nitration of 4-methylquinoline (**1**) and methyl quinoline-4-carboxylate (**5**) in the 8-position resulting in 4-methy-8-nitroquinoline (**2**) and methyl 8-nitroquinoline-4-carboxylate (**6**) (Scheme 1).<sup>24</sup> **5** was obtained in a preceding step by esterification of quinoline-4-carboxylic acid (**4**). Afterward, **2** and **6** were reduced with hydrogen using Pd/C as catalyst yielding the amine precursors 4-methy-8-aminoquinoline (**3**) and methyl 8-aminoquinoline-2-carboxylate (**7**).<sup>25</sup> In the last step, the reaction of **3** and **7** with the Vilsmeier salt *N,N,N',N'*-tetramethylchloroformamidinium chloride (TMG-VS) resulted in **L7** and **L8** analogously to the procedure reported earlier.<sup>26</sup> The molecular structure of **L7** in the solid state was determined by SCXRD (molecular structure and crystallographic data are provided in Fig. S1 and Table S1 in the ESI†).

### Influence of the substituents on the electronic properties of the ligands

Density functional theory (DFT) calculations were performed for **L7** and **L8** applying the functional TPSSH and the basis set def2-TZVP with a solvent model for MeCN using the polarizable continuum model (PCM) and an empirical dispersion correction using the D3 version of Grimme's dispersion with Becke-Johnson damping (GD3BJ) (further information in the ESI†).<sup>27–34</sup> This combination was chosen because previous studies showed very good results for comparable systems.<sup>20–23,34–37</sup> After structural optimization calculations, natural bond orbital (NBO) calculations were executed to analyze the substituent influence on the guanidine N donor  $N_{\text{gua}}$  and quinolinyl N donor  $N_{\text{qu}}$  of both ligands and the acyl O atom  $O_{\text{acyl}}$  and alcohol O atom  $O_{\text{alc}}$  of the methyl ester substituent of **L8**. The results of **L7** and **L8** are compared with the results of **L1**, **L2** and **L5** from the previous study (Fig. 2).<sup>23</sup>

The NBO charge of the  $N_{\text{gua}}$  donor is not affected by the substitutions entailing that the basicity of the  $N_{\text{gua}}$  donor is not affected electronically. Since the same donor type is discussed, this result indicates that the donor strength of the  $N_{\text{gua}}$  is also

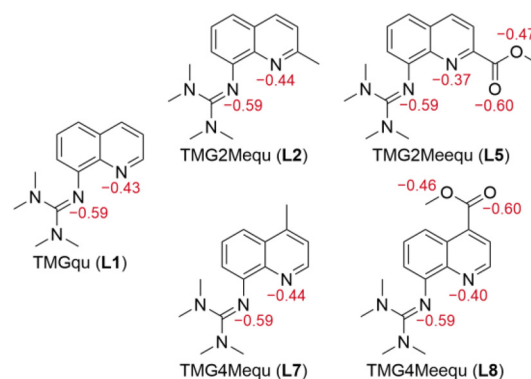
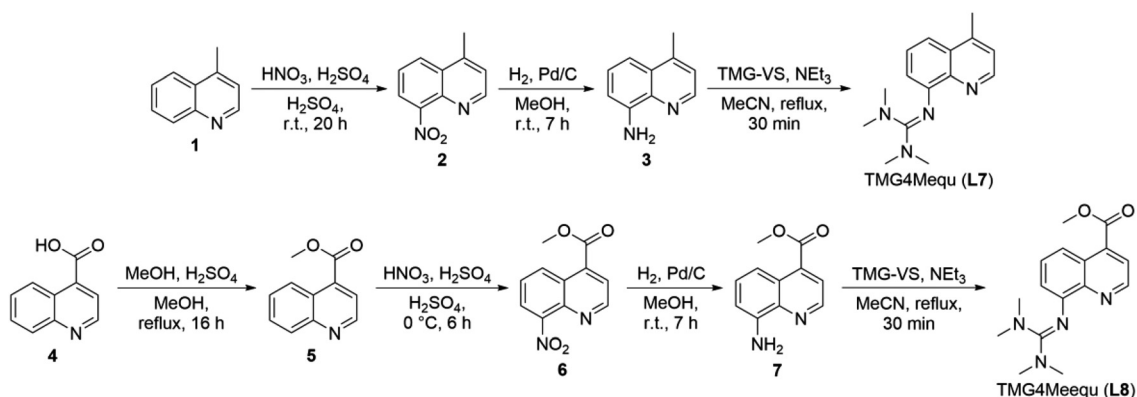


Fig. 2 Calculated NBO charges (in e units, red) of the  $N_{\text{gua}}$  and  $N_{\text{qu}}$  donor atoms of **L1**,<sup>21</sup> **L2**,<sup>21</sup> **L5**,<sup>21</sup> **L7** and **L8** and of the  $O_{\text{acyl}}$  and  $O_{\text{alc}}$  atoms of **L5** and **L7** (NBO6.0, TPSSH, def2-TZVP, GD3BJ, PCM (MeCN)).

not affected by the substituents. Further, the NBO charge of the  $N_{\text{gua}}$  donor is more negative than the NBO charge of the  $N_{\text{qu}}$  donor indicating a higher basicity of the  $N_{\text{gua}}$  donor. However, since NBO charges only correlate with basicity and different donor types are compared this does not imply that the  $N_{\text{gua}}$  donor is a stronger donor than the  $N_{\text{qu}}$  donor.<sup>20,23,25,35,37,38</sup> The basicity and possible donor strength of the  $N_{\text{qu}}$  donor of **L2** and **L7** are not significantly affected by the weak electronic influence of the alkyl substituents. In contrast, the strong electron density withdrawing effect of the methyl ester substituents of **L5** and **L8** leads to an increase of the NBO charge of the  $N_{\text{qu}}$  donor in comparison to the unsubstituted ligand. Therefore, the basicity and the possible donor strength of the  $N_{\text{qu}}$  donor are decreased. However, the effect of the methyl ester substituent in the 2-position of **L5** is stronger than in the 4-position of **L8**. The NBO charges of the  $O_{\text{acyl}}$  and  $O_{\text{alc}}$  atoms are not affected by the position of the methyl ester substituent.

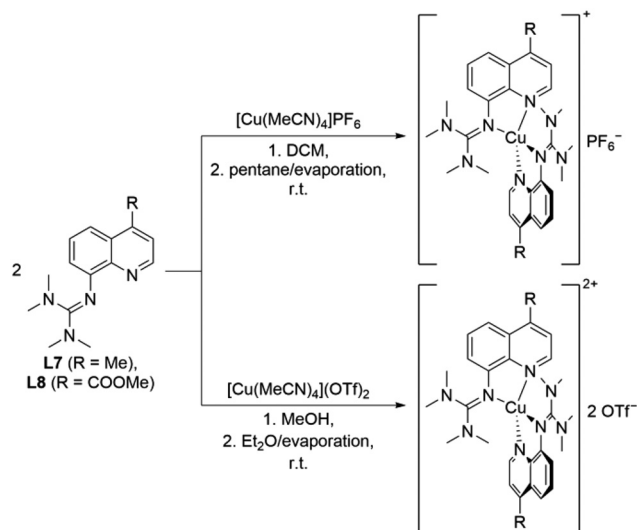
### Synthesis and structural characterization of the copper complexes

The reaction of two equivalents of **L7** or **L8** with Cu(I) or Cu(II) salts with weakly coordinating anions resulted in the corres-



Scheme 1 Synthetic routes for the synthesis of TMG4Mequ (**L7**) (top) and TMG4Meequ (**L8**) (bottom).

ponding bis(chelate) Cu(I) and Cu(II) complexes. The Cu(I) complexes were crystallized by dissolving **L7** or **L8** and  $[\text{Cu}(\text{MeCN})_4]\text{PF}_6$  in DCM followed by layering with pentane or slow evaporation of the solvent (Scheme 2, top). The Cu(II) complexes were crystallized similarly by dissolving **L7** or **L8** and  $[\text{Cu}(\text{MeCN})_4](\text{OTf})_2$  in MeOH followed by layering with  $\text{Et}_2\text{O}$  or slow evaporation of the solvent (Scheme 2, bottom). The complex cations  $[\text{Cu}(\text{TMG4Mequ})_2]^+$  (**C11**),  $[\text{Cu}(\text{TMG4Mequ})_2(\text{OTf})]^+$  (**C12+OTf**),  $[\text{Cu}(\text{TMG4Meequ})_2]^+$  (**C13**) and  $[\text{Cu}(\text{TMG4Meequ})_2]^{2+}$  (**C14**) were structurally characterized by SCXRD measurements (Fig. 3) of the crystallized compounds **C11-PF<sub>6</sub>**, **(C12+OTf)-OTf**, **C13-PF<sub>6</sub>** and **C14-OTf** (molecular structures in the solid state and crystallographic data are shown in Fig. S2–S5 and Tables S1, S2 in the ESI†).



**Scheme 2** Synthesis of the Cu(I) (top) and Cu(II) (bottom) compounds **C11–X–C14–X**.

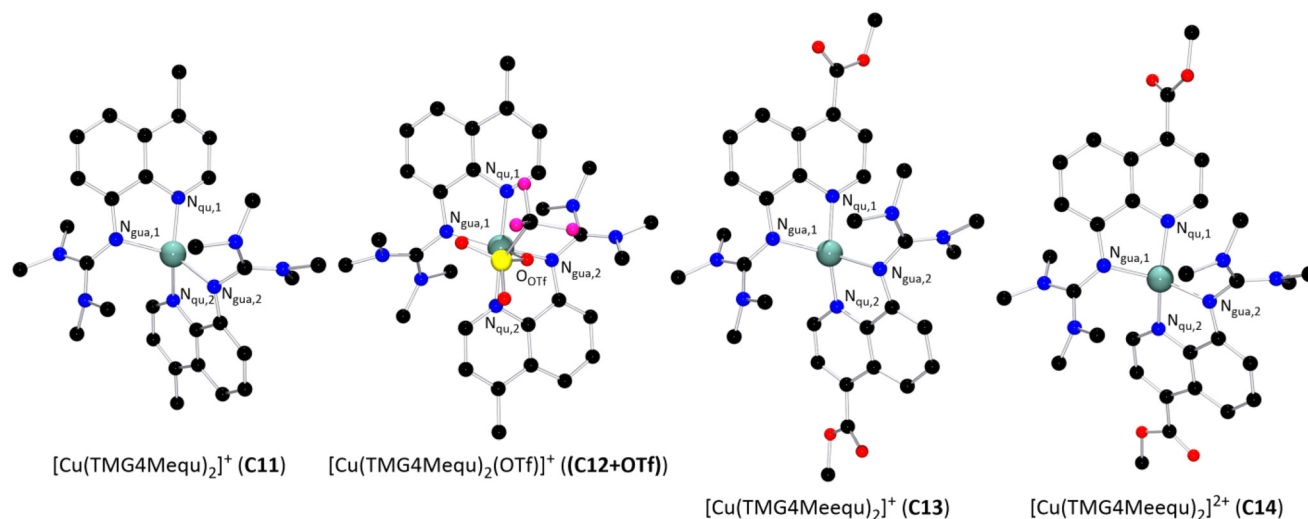


**Fig. 3** Molecular structures of the Cu(I) and Cu(II) complex cations **C11–C14** in crystals of **C11–X–C14–X** (H atoms, non-coordinating anions and solvent molecules are omitted for clarity).

**C11–PF<sub>6</sub>** possesses two independent molecules in the unit cell which are very similar (Table S3 in the ESI†). Therefore, only one independent molecule is discussed in the following. Important bond lengths, bond angles and structure parameters of the copper complex cations **C11–C14** are compared with those of  $[\text{Cu}(\text{TMGqu})_2]^+$  (**C1**),  $[\text{Cu}(\text{TMGqu})_2]^{2+}$  (**C2**),  $[\text{Cu}(\text{TMG2Mequ})_2]^+$  (**C3**),  $[\text{Cu}(\text{TMG2Mequ})_2]^{2+}$  (**C4**),  $[\text{Cu}(\text{TMG2Meequ})_2]^+$  (**C7**) and  $[\text{Cu}(\text{TMG2Mequ})_2]^{2+}$  (**C8**) of the crystallized compounds **C1–PF<sub>6</sub>**, **C2–OTf**, **C3–PF<sub>6</sub>**, **C4–BF<sub>4</sub>**, **C7–PF<sub>6</sub>** and **C8–BF<sub>4</sub>** of previous studies (Table 1).<sup>19,23</sup>

The geometry of the coordination sphere around the metal center is described by the  $\tau_4$  parameter and the plane angle  $\angle$  between the planes stretched by the two N donors of each ligand and the copper center.<sup>39</sup> In the case of **(C12+OTf)**, the weakly coordinating triflate is not considered for the calculation of the  $\tau_4$  parameter because the previous study emphasized that the weak coordination of a triflate has no significant influence on the  $\tau_4$  parameter.<sup>23</sup> The  $\tau_4$  value enables the characterization between an ideal square-planar ( $\tau_4 = 0$ ) or ideal tetrahedral ( $\tau_4 = 1$ ) coordination geometry. The average coordination geometry of the related Cu(I) and Cu(II) complexes is described by the  $\bar{\tau}_4$  parameter, which is the mean of the  $\tau_4$  parameters of the related Cu(I) and Cu(II) complexes. The similarity between the coordination geometry of the related Cu(I) and Cu(II) complexes is described by the  $\Delta\tau_4$  parameter and plane angle difference  $\Delta\angle$ , which are the difference between the  $\tau_4$  parameters and the plane angles  $\angle$  of the related Cu(I) and Cu(II) complexes, respectively. To describe the similarity between the whole structures of the related Cu(I) and Cu(II) complexes, the root-mean-square deviation (RMSD) is applied.<sup>40</sup>

In general, all complexes are highly distorted from an ideal coordination geometry indicated by  $\tau_4$  values clearly deviating from 0 or 1. The Cu(I) complex cations possess higher  $\tau_4$  values ( $\tau_4 = 0.57$  to  $0.67$ ) compared to the corresponding Cu(II)





**Table 1** Selected bond lengths, bond angles and structure parameters of [Cu(TMGqu)<sub>2</sub>]<sup>+</sup> (**C1**),<sup>19</sup> [Cu(TMGqu)<sub>2</sub>]<sup>2+</sup> (**C2**),<sup>19</sup> [Cu(TMG2Mequ)<sub>2</sub>]<sup>+</sup> (**C3**),<sup>23</sup> [Cu(TMG2Mequ)<sub>2</sub>]<sup>2+</sup> (**C4**),<sup>23</sup> [Cu(TMG2Meequ)<sub>2</sub>]<sup>+</sup> (**C7**),<sup>23</sup> [Cu(TMG2Meequ)<sub>2</sub>]<sup>2+</sup> (**C8**),<sup>23</sup> [Cu(TMG4Mequ)<sub>2</sub>]<sup>+</sup> (**C11**), [Cu(TMG4Mequ)<sub>2</sub>(OTf)]<sup>+</sup> ((**C12** + OTf)), [Cu(TMG4Meequ)<sub>2</sub>]<sup>+</sup> (**C13**) and [Cu(TMG4Meequ)<sub>2</sub>]<sup>2+</sup> (**C14**)

	[Cu(TMGqu) <sub>2</sub> ] <sup>+/2+</sup>		[Cu(TMG2Mequ) <sub>2</sub> ] <sup>+/2+</sup>		[Cu(TMG2Meequ) <sub>2</sub> ] <sup>+/2+</sup>		[Cu(TMG4Mequ) <sub>2</sub> ] <sup>+/2+</sup>		[Cu(TMG4Meequ) <sub>2</sub> ] <sup>+/2+</sup>	
	<b>C1</b> (Cu(I))	<b>C2</b> (Cu(II))	<b>C3</b> (Cu(I))	<b>C4</b> (Cu(II))	<b>C7</b> (Cu(I))	<b>C8</b> (Cu(II))	<b>C11</b> (Cu(I))	<b>(C12+OTf)</b> (Cu(II))	<b>C13</b> (Cu(I))	<b>C14</b> (Cu(II))
Bond lengths [Å]										
Cu–N <sub>gua</sub> ,1/2	2.068(3), 2.095(3)	1.959(2), 1.964(2)	2.091(3), 2.097(3)	1.979(4), 1.978(4)	2.047(4), 2.029(4)	2.039(2), 2.043(2)	2.082(3), 2.055(3)	1.987(3), 1.994(3)	2.056(2), 2.063(2)	1.969(2), 1.953(2)
Cu–N <sub>qu</sub> ,1/2	1.966(4), 1.999(3)	1.976(2), 1.975(2)	1.994(3), 1.994(3)	1.987(4), 1.972(4)	2.053(3), 2.083(4)	1.960(2), 1.959(2)	1.970(3), 1.993(3)	1.988(3), 1.977(3)	2.003(2), 1.987(2)	1.969(2), 1.979(2)
Cu–O <sub>acyl</sub> ,1/2					2.962(4), 4.312(4)	2.616(2), 2.595(2)				
Cu–O <sub>alc</sub> ,1/2					4.511(4), 3.235(4)	4.428(2), 4.441(2)				
Cu–OTf								2.444(3)		
Bond angles [°]										
N <sub>gua</sub> ,1/2–Cu–N <sub>qu</sub> ,1/2	82.6(2), 82.1(2)	83.5(1), 83.7(1)	81.7(2), 81.6(2)	83.2(2), 83.6(2)	81.3(2), 81.3(2)	82.2(1), 82.2(1)	82.8(2), 82.5(2)	82.2(2), 82.6(2)	81.7(1), 81.8(1)	83.8(1), 83.3(1)
N <sub>gua</sub> ,1–Cu–N <sub>gua</sub> ,2	129.1(2)	149.4(1)	126.0(2)	135.9(2)	124.4(2)	120.2(1)	127.5(2)	144.5(2)	133.8(1)	147.5(1)
N <sub>gua</sub> ,1/2–Cu–N <sub>qu</sub> ,2/1	108.2(2), 114.1(2)	102.6(1), 103.5(1)	111.7(2), 113.2(2)	105.4(2), 107.2(2)	133.0(2), 137.8(2)	105.3(1), 106.9(1)	111.3(2), 120.9(2)	101.9(2), 102.2(2)	115.9(1), 107.3(1)	104.1(1), 104.5(1)
N <sub>qu</sub> ,1–Cu–N <sub>qu</sub> ,2	149.0(2)	154.9(1)	149.9(2)	154.6(2)	105.9(2)	163.7(1)	138.1(2)	165.6(2)	146.2(1)	152.4(1)
Structure parameters										
τ <sub>4</sub> [°] <sup>a</sup>	0.58	0.40	0.60	0.49	0.63	0.54 <sup>b</sup>	0.67 <sup>c</sup>	0.35	0.57	0.43
∠τ <sub>4</sub> [°]		0.49		0.54		0.59 <sup>b</sup>		0.51		0.50
Δτ <sub>4</sub> [°]		0.18		0.10		0.09 <sup>b</sup>		0.32		0.14
Δ (CuN <sub>2</sub> , CuN' <sub>2</sub> ) [°]	65.1	42.5	68.2	54.7	69.0	65.6 <sup>b</sup>	74.2	40.8	63.0	45.9
ΔΔ [°]		22.6		13.5		3.5 <sup>b</sup>		33.5		17.1
RMSD [Å]		0.346		0.153		2.283		0.529		0.532

<sup>a</sup>  $\tau_4 = \frac{360^\circ - (\alpha + \beta)}{141^\circ}$ .<sup>29</sup> <sup>b</sup> The comparability of this value is limited due to the 4 + 2 coordination motif. <sup>c</sup> The weakly coordinating triflate is not considered.

complex cations ( $\tau_4 = 0.35$  to  $0.54$ ) because Cu(I) prefers a tetrahedral and Cu(II) a square-planar coordination geometry.<sup>14</sup> Regarding the Cu–N<sub>gua</sub> and Cu–N<sub>qu</sub> bond lengths, they are comparable among the Cu(I) complexes **C1**, **C3**, **C11** and **C13** and among the Cu(II) complexes **C2**, **C4**, (**C12+OTf**) and **C14**. In the Cu(I) complexes **C1**, **C3**, **C11** and **C13**, the Cu–N<sub>qu</sub> bond lengths are significantly shorter than the Cu–N<sub>gua</sub> bond lengths whereas the Cu–N<sub>gua</sub> and Cu–N<sub>qu</sub> bond lengths are more similar in the Cu(II) complexes **C2**, **C4**, (**C12+OTf**) and **C14**. Therefore, the methyl substituent in the 2- or 4-position or the methyl ester substituent in the 4-position have no significant influence on the bond lengths of **C2**, **C3**, **C11**, (**C12+OTf**), **C13** and **C14** compared to the unsubstituted **C1** and **C2**. The  $\tau_4$  values and bond lengths of **C7** and **C8** are not comparable with the other complexes due to the significant influence of the methyl ester substituent.<sup>23</sup>

In the previous study, we found that the methyl substituent in the 2-position of **L2** increases the  $\tau_4$  parameters of **C3** and **C4** compared to **C1** and **C2** and, therefore, also the  $\angle\tau_4$  parameter of **C3** and **C4**. In addition, the coordination geometries and structures of **C3** and **C4** possess a higher similarity indicated by the smaller  $\Delta\tau_4$  parameter, plane angle difference  $\Delta\Delta$  and RMSD of **C3** and **C4** compared to **C1** and **C2**. We substantiated these effects with the steric demand of the methyl substituent and not with an electronic effect since the methyl substituent only induces a weak electronic influence.<sup>23</sup> The results of **C11** and (**C12+OTf**) prove this argumentation because the

observed structural effects in **C3** and **C4** compared to **C1** and **C2** are not visible in **C11** and (**C12+OTf**). However, the  $\tau_4$  parameters of **C11** and (**C12+OTf**) differ significantly from those of **C1** and **C2** which is probably caused by packing effects and the weak coordination of the triflate in (**C12+OTf**) (see discussion of the DFT results). Due to the 4-position of the methyl substituent, the electronic effect on the N<sub>qu</sub> donor of **L7** is similar to that of the methyl substituent in the 2-position of **L2** (see discussion of the NBO results of the ligands). Therefore, the steric demand of the methyl substituent in the 2-position of **L2** is proven to be the reason for the particular structural properties of **C3** and **C4**.

Further, we discovered that the methyl ester substituent in the 2-position of **L5** induces a substantial difference in the structures in **C7** and **C8** compared to all other related Cu(I) and Cu(II) complexes indicated by the high RMSD. We constituted the elongated Cu–N<sub>qu</sub> bond length in **C7** compared to **C1** with the weakened donor properties of the N<sub>qu</sub> donor in **C7** induced by the electron density withdrawing effect and the steric demand of the methyl ester substituent.<sup>23</sup> However, no elongation of the Cu–N<sub>qu</sub> bond length is present in **C13** which entails that the elongation in **C7** is not caused by the electron density withdrawing effect but just by the steric demand. In **C8**, we observed a 4 + 2 coordination motif due to the donor properties of the methyl ester substituent in the 2-position.<sup>23</sup> This coordination motif is not possible in **C14** resulting in a significantly higher structural similarity between **C13** and **C14** compared to **C7** and **C8**.



The results show that the 2-position is crucial for the substituent influence on the complex structures because the structural particularities of **C3**, **C4**, **C7** and **C8** are not present in **C11–C14**. Therefore, the investigation of **C11–C14** enables the analysis of the pure electronic effect of the methyl and methyl ester substituent without the influence of a steric demand or additional donor properties.

### DFT calculations of the copper complexes

DFT calculations for **C11–C14** were performed analogously to the DFT calculations for **L7** and **L8** (further information in the ESI†).<sup>27–34</sup> In the case of **C12**, the weakly coordinating triflate present in the molecular structure of (**C12**+OTf) was not considered for the calculations. First, optimization calculations were performed (Table 2, more structural information are provided in Tables S4 and S5 in the ESI†). In general, the com-

plexes possess a high agreement between the molecular structures in the solid state and the calculated structures.

Following the optimization calculations, NBO calculations were performed for **C11–C14** to investigate the substituent influence on the NBO charges of the copper center caused by the methyl ester substituent. In the previous study, we argued that the  $N_{qu}$  donor in **C7** is affected by the steric demand and electron density withdrawing effect of the methyl ester substituent.<sup>23</sup> However, the results of **C13** show that the influence of the methyl ester substituent in **C7** is thus limited to the steric demand.

Contrary to the Cu(I) complexes, the substituent influence on the  $N_{gua}$  and  $N_{qu}$  donor is more noticeable in the Cu(II) complexes (Fig. 4, bottom). In **C4**, a significant weakening of the donor properties of the  $N_{gua}$  donor, revealed by the substantially decreased charge-transfer energy compared to **C2**, is

**Table 2** Overview of the discussed ligands, complex cations and redox couples

Ligand (label)	Complex cation (label)	Complex redox couple (label)
TMGqu ( <b>L1</b> )	[Cu(TMGuqu) <sub>2</sub> ] <sup>+</sup> ( <b>C1</b> ) [Cu(TMGuqu) <sub>2</sub> ] <sup>2+</sup> ( <b>C2</b> )	[Cu(TMGuqu) <sub>2</sub> ] <sup>+2+</sup> ( <b>R1</b> )
TMG2Mequ ( <b>L2</b> )	[Cu(TMGu2Mequ) <sub>2</sub> ] <sup>+</sup> ( <b>C3</b> ) [Cu(TMGu2Mequ) <sub>2</sub> ] <sup>2+</sup> ( <b>C4</b> )	[Cu(TMGu2Mequ) <sub>2</sub> ] <sup>+2+</sup> ( <b>R2</b> )
TMG2 <sup>6</sup> Hexqu ( <b>L4</b> )	[Cu(TMGu2 <sup>6</sup> Hexqu) <sub>2</sub> ] <sup>+</sup> ( <b>C5</b> ) [Cu(TMGu2 <sup>6</sup> Hexqu) <sub>2</sub> ] <sup>2+</sup> ( <b>C6</b> )	[Cu(TMGu2 <sup>6</sup> Hexqu) <sub>2</sub> ] <sup>+2+</sup> ( <b>R3</b> )
TMG2Meequ ( <b>L5</b> )	[Cu(TMGu2Meequ) <sub>2</sub> ] <sup>+</sup> ( <b>C7</b> ) [Cu(TMGu2Meequ) <sub>2</sub> ] <sup>2+</sup> ( <b>C8</b> )	[Cu(TMGu2Meequ) <sub>2</sub> ] <sup>+2+</sup> ( <b>R4</b> )
TMG4NMe <sub>2</sub> qu ( <b>L6</b> )	[Cu(TMGu4NMe <sub>2</sub> qu) <sub>2</sub> ] <sup>+</sup> ( <b>C9</b> ) [Cu(TMGu4NMe <sub>2</sub> qu) <sub>2</sub> ] <sup>2+</sup> ( <b>C10</b> )	[Cu(TMGu4NMe <sub>2</sub> qu) <sub>2</sub> ] <sup>+2+</sup> ( <b>R5</b> )
TMG4Mequ ( <b>L7</b> )	[Cu(TMGu4Mequ) <sub>2</sub> ] <sup>+</sup> ( <b>C11</b> ) [Cu(TMGu4Mequ) <sub>2</sub> ] <sup>2+</sup> ( <b>C12</b> )	[Cu(TMGu4Mequ) <sub>2</sub> ] <sup>+2+</sup> ( <b>R6</b> )
TMG4Meequ ( <b>L8</b> )	[Cu(TMGu4Meequ) <sub>2</sub> ] <sup>+</sup> ( <b>C13</b> ) [Cu(TMGu4Meequ) <sub>2</sub> ] <sup>2+</sup> ( <b>C14</b> )	[Cu(TMGu4Meequ) <sub>2</sub> ] <sup>+2+</sup> ( <b>R7</b> )

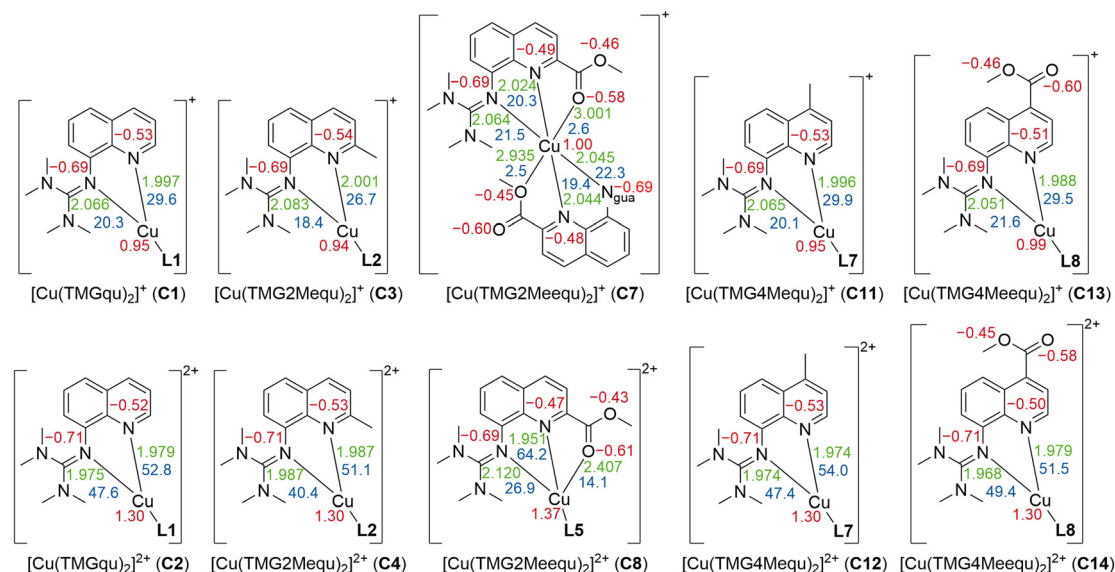


**Fig. 4** Selected calculated NBO charges [e units] (red), charge-transfer energies  $E_{CT}$  [kcal mol<sup>-1</sup>] (blue) and bond length [Å] (green) of the Cu(I) (top) and Cu(II) (bottom) complex cations **C1–C4**,<sup>23</sup> **C7**,<sup>23</sup> **C8**<sup>23</sup> and **C11–C14** (in case of nonexistent or insignificant differences between both ligands, the average values are presented and the coordination of one bidentate ligand is simplified; NBO6.0, TPSSH, def2-TZVP, GD3BJ, PCM (MeCN); all values are provided in Table S6 and S7 in the ESI†).



present. Since this effect on the  $N_{\text{gua}}$  donor does not occur in **C12**, the steric demand of the methyl substituent in the 2-position is responsible for the effect in **C4**. The results of **C14** show that the extraordinary long  $\text{Cu}-N_{\text{gua}}$  bond length and weak donor properties of the  $N_{\text{gua}}$  donor in **C8** compared to **C2** are a result of the 4 + 2 coordination motif present in **C8** and not of a possible electronic influence of the methyl ester substituent on the  $N_{\text{gua}}$  donor. The  $N_{\text{qu}}$  donor in **C12** and **C14** is affected in the opposite way by the substituents compared to the  $N_{\text{qu}}$  donor in **C4** and **C8**. In **C4**, the steric demand of the methyl substituent elongates the  $\text{Cu}-N_{\text{qu}}$  bond length resulting in a lower charge-transfer energy and, therefore, weaker donor properties of the  $N_{\text{qu}}$  donor compared to **C2**. In contrast, the weak electron density donating effect of the methyl substituent induces a higher charge-transfer energy and, therefore, increased donor strength of the  $N_{\text{qu}}$  donor in **C12** compared to **C2**. In **C8**, the pulling effect of the  $O_{\text{acyl}}$  donor on the  $\text{Cu(II)}$  center, induced by the 4 + 2 coordination motif, shortens the  $\text{Cu}-N_{\text{qu}}$  bond length compared to **C2** leading to a significantly increased charge-transfer energy of the  $N_{\text{qu}}$  donor. If this pulling effect of the methyl ester substituent is not present as in **C14**, only the electron density withdrawing effect on the  $N_{\text{qu}}$  donor remains. Therefore, the charge-transfer energy of the  $N_{\text{qu}}$  donor is decreased in **C14** compared to **C2**. These results

demonstrate that in **C8** the strengthening of the  $N_{\text{qu}}$  donor induced by the pulling effect of the methyl ester substituent on the  $\text{Cu(II)}$  center overcomes the weakening of the  $N_{\text{qu}}$  donor caused by the electron density withdrawing effect of the methyl ester substituent. Regarding all complexes **C1–C14** (Table 2), the substituent influence results in different correlations between the charge-transfer energy and the bond length in dependency of the donor and the oxidation state of the copper center (Fig. 5).

Since the substituents affect the donor properties of the  $N_{\text{gua}}$  and  $N_{\text{qu}}$  donor, they also affect the total donor properties of the ligands. The total donor properties of the ligands are described by the total charge-transfer energy  $E_{\text{CT,total}}$  which is the sum of the charge-transfer energies  $E_{\text{CT,gua}}$  and  $E_{\text{CT,qu}}$  of the  $N_{\text{gua}}$  and  $N_{\text{qu}}$  donor (values provided in Table S8 in the ESI†). Due to the donor properties of the methyl ester substituent in the 2-position, a second value for the total charge-transfer energy  $E_{\text{CT,total}}$  of **C7** and **C8** considering the charge-transfer energies of the O donors is defined. The different donor properties influence the theoretical stabilization of the copper complexes quantified by the ground state energies  $E_{\text{GS,DFT}}$  of the copper complexes. To enable the relative comparison of the different substituent influences on the donor properties and, therefore, on the theoretical stabilization of the related  $\text{Cu(I)}$  and  $\text{Cu(II)}$  complexes, the related  $\text{Cu(I)}$  and  $\text{Cu(II)}$  complexes **C1–C14** are regarded as the copper complex redox couples **R1–R7** (Table 2). This leads to the calculation of the charge-transfer energy differences  $\Delta E_{\text{CT,total}}$ ,  $\Delta E_{\text{CT,gua}}$  and  $\Delta E_{\text{CT,qu}}$  between the related  $\text{Cu(I)}$  and  $\text{Cu(II)}$  complexes (eqn (1), values provided in Table S8 in the ESI†).

$$\Delta E_{\text{CT,donor}}(\text{RX}) = E_{\text{CT,donor}}(\text{Cu(II)}(\text{RX})) - E_{\text{CT,donor}}(\text{Cu(I)}(\text{RX})) \quad (1)$$

Then, the differences  $\Delta \Delta E_{\text{CT,total}}$ ,  $\Delta \Delta E_{\text{CT,gua}}$  and  $\Delta \Delta E_{\text{CT,qu}}$  between the charge-transfer energy differences  $\Delta E_{\text{CT,total}}$ ,  $\Delta E_{\text{CT,gua}}$  and  $\Delta E_{\text{CT,qu}}$  of the redox couples and **R1** are calculated (eqn (2) and Table 3). These values, referred to as referenced total charge-transfer energy differences  $\Delta \Delta E_{\text{CT,total}}$ , describe whether a substituent induces a relatively better donation in the  $\text{Cu(I)}$  or  $\text{Cu(II)}$  species of a redox couple compared to **R1**. A relatively better donation of the  $\text{Cu(I)}$  species of a redox couple compared to **R1** is indicated by a positive  $\Delta \Delta E_{\text{CT,total}}$ ,  $\Delta \Delta E_{\text{CT,gua}}$  and  $\Delta \Delta E_{\text{CT,qu}}$  value and a relatively better donation of the  $\text{Cu(II)}$  species of a redox couple com-

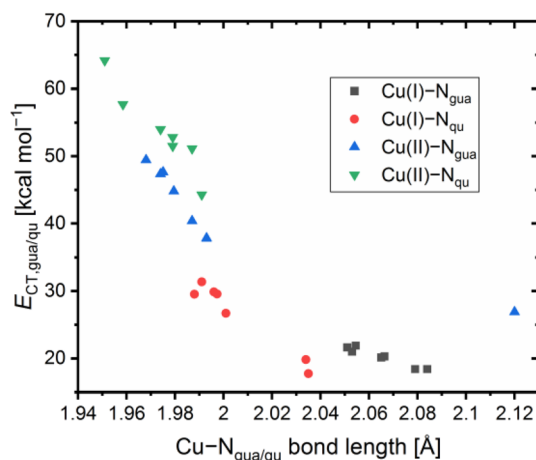


Fig. 5 Plot of the charge-transfer energies  $E_{\text{CT}}$  of the  $N_{\text{gua}}$  and  $N_{\text{qu}}$  donor to the Cu center against the  $\text{Cu}-N_{\text{gua}}$  and  $\text{Cu}-N_{\text{qu}}$  bond lengths of **C1–C14** (in case the two ligands exhibit different values for the same type of donor, the average value is used).

Table 3 Calculated  $\Delta \Delta E_{\text{CT,total}}$  ( $\Delta \Delta E_{\text{CT,total}}$  value of **R4** that includes the O donors is marked in red),  $\Delta \Delta E_{\text{CT,gua}}$ ,  $\Delta \Delta E_{\text{CT,qu}}$  and  $\Delta \Delta E_{\text{GS,DFT}}$  values of **R1–R7** (NBO6.0, TPSSH, def2-TZVP, GD3BJ, PCM (MeCN))

	$\Delta \Delta E_{\text{CT,total}}$ [kcal mol <sup>−1</sup> ]	$\Delta \Delta E_{\text{CT,gua}}$ [kcal mol <sup>−1</sup> ]	$\Delta \Delta E_{\text{CT,qu}}$ [kcal mol <sup>−1</sup> ]	$\Delta \Delta E_{\text{GS}}$ [kJ mol <sup>−1</sup> ]
$[\text{Cu}(\text{TMGqu})_2]^{+/2+}$ ( <b>R1</b> )	0.0	0.0	0.0	0.0
$[\text{Cu}(\text{TMG2Mequ})_2]^{+/2+}$ ( <b>R2</b> )	−8.5	−10.7	2.2	12.7
$[\text{Cu}(\text{TMG2}^{\text{c}}\text{Hexqu})_2]^{+/2+}$ ( <b>R3</b> )	−14.5	−21.0	6.5	23.3
$[\text{Cu}(\text{TMG2Meequ})_2]^{+/2+}$ ( <b>R4</b> )	−2.5 (20.4)	−44.7	42.1	−1.2
$[\text{Cu}(\text{TMG4NMe}_2\text{qu})_2]^{+/2+}$ ( <b>R5</b> )	4.2	−1.9	6.1	−28.4
$[\text{Cu}(\text{TMG4Mequ})_2]^{+/2+}$ ( <b>R6</b> )	1.4	−0.3	1.7	−6.4
$[\text{Cu}(\text{TMG4Meequ})_2]^{+/2+}$ ( <b>R7</b> )	−1.7	0.9	−2.6	14.9

pared to **R1** is indicated by a negative  $\Delta\Delta E_{\text{CT,total}}$ ,  $\Delta\Delta E_{\text{CT,gua}}$  and  $\Delta\Delta E_{\text{CT,qu}}$  value.

$$\Delta\Delta E_{\text{CT,donor}}(\text{RX}) = \Delta E_{\text{CT,donor}}(\text{RX}) - \Delta E_{\text{CT,donor}}(\text{R1}) \quad (2)$$

In an analogous procedure, the referenced ground state energy differences  $\Delta\Delta E_{\text{GS,DFT}}$  of the redox couples are calculated (eqn (3), (4) and Table 3,  $E_{\text{GS,DFT}}$  and  $\Delta E_{\text{GS,DFT}}$  values provided in Table S9 in the ESI†). These values describe whether a substituent induces a relatively better theoretical stabilization of the Cu(i) or Cu(ii) species of a redox couple compared to **R1**. A relatively better theoretical stabilization of the Cu(i) species of a redox couple compared to **R1** is indicated by a negative  $\Delta\Delta E_{\text{GS,DFT}}$  value and a relatively better donation of the Cu(ii) species of a redox couple compared to **R1** is indicated by a positive  $\Delta\Delta E_{\text{GS,DFT}}$  value.

$$\Delta E_{\text{GS}}(\text{RX}) = E_{\text{GS}}(\text{Cu(II)}(\text{RX})) - E_{\text{GS}}(\text{Cu(I)}(\text{RX})) \quad (3)$$

$$\Delta\Delta E_{\text{GS}}(\text{RX}) = \Delta E_{\text{GS}}(\text{RX}) - \Delta E_{\text{GS}}(\text{R1}) \quad (4)$$

The results demonstrate that the referenced total charge-transfer energy differences  $\Delta\Delta E_{\text{CT,total}}$  and referenced ground state energy differences  $\Delta\Delta E_{\text{GS,DFT}}$  correlate with each other except for **R4** (Fig. 6). For **R2**, **R3** and **R7**, the relatively stronger total donation in the Cu(i) species compared to **R1**, indicated by a negative  $\Delta\Delta E_{\text{CT,total}}$  value, leads to a relatively better theoretical stabilization of the Cu(i) species compared to **R1**, indicated by a positive  $\Delta\Delta E_{\text{GS,DFT}}$  value. The opposite case occurs for **R5** and **R7**. Therefore, the relative theoretical stabilization can be estimated based on the relative total donor properties of the ligands.

Furthermore, two different linear correlations between the referenced total charge-transfer energy difference  $\Delta\Delta E_{\text{CT,total}}$  and the referenced ground state energy difference  $\Delta\Delta E_{\text{GS}}$ ,

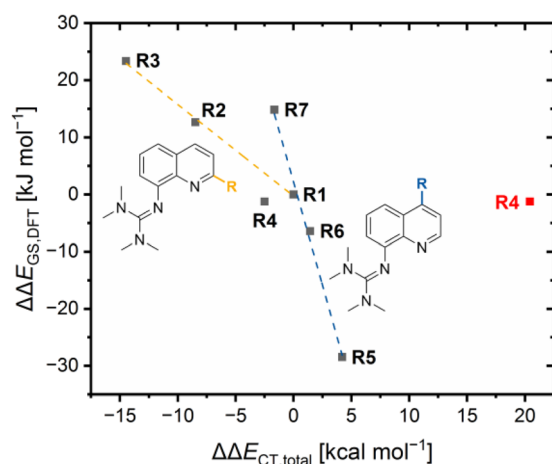


Fig. 6 Plot of the referenced ground state energy differences  $\Delta\Delta E_{\text{GS,DFT}}$  against the referenced total charge-transfer energy differences  $\Delta\Delta E_{\text{CT,total}}$  of **R1**–**R7** (yellow correlation considers **R1** and in 2-position alkyl-substituted redox couples, blue correlation considers **R1** and in 4-position substituted redox couples, data point of **R4** that also considers the O donors is marked red).

depending on the substituent position, are present. **R2** and **R3** with alkyl substituents in the 2-position and **R1** form one correlation and **R5**, **R6** and **R7** with substituents in the 4-position and **R1** form the other. The reason for the two linear correlations is the different ways the substituents in the 2- and 4-position affect the relative donor properties of the  $N_{\text{gua}}$  and  $N_{\text{qu}}$  donor represented by the referenced charge-transfer energy differences of the guanidine and quinoline donor  $\Delta\Delta E_{\text{CT,gua}}$  and  $\Delta\Delta E_{\text{CT,qu}}$  (Table 3). In **R2** and **R3**, the steric demand of the alkyl substituents in the 2-position affects the  $N_{\text{gua}}$  and  $N_{\text{qu}}$  in opposite ways. Whereas the  $N_{\text{gua}}$  donor possesses a relatively stronger donation in the Cu(i) species of **R2** and **R3** compared to **R1**, indicated by positive  $\Delta\Delta E_{\text{CT,qu}}$  values, the  $N_{\text{qu}}$  donor possesses a relatively stronger donation in the Cu(ii) species, indicated by negative  $\Delta\Delta E_{\text{CT,gua}}$  values. However, the relative donor strength of the  $N_{\text{gua}}$  donor is significantly more affected than that of the  $N_{\text{qu}}$  donor. Therefore, the influence on the  $N_{\text{gua}}$  donor prevails that on the  $N_{\text{qu}}$  donor. The prevailing influence on the donor properties of the  $N_{\text{gua}}$  donor increases with the steric demand ( $\text{H} < \text{Me} < \text{Hex}$ ). For this reason, the  $\Delta\Delta E_{\text{CT,total}}$  values decrease with the steric demand, indicating a relatively stronger donation of the Cu(i) species.

Contrary effects on the  $N_{\text{gua}}$  and  $N_{\text{qu}}$  donor, like in **R2**–**R3**, are also visible for **R5**–**R7**. However, in these cases the relative donor properties of the  $N_{\text{qu}}$  donor is more affected than that of the  $N_{\text{gua}}$  donor and, hence, the influence on the  $N_{\text{qu}}$  donor prevails that on the  $N_{\text{gua}}$  donor. The reason is, that the substituents in the 4-position only possess an electronic influence which mainly affects the  $N_{\text{qu}}$  donor but no steric demand that could influence the coordination geometry and, therefore, the donor properties of the  $N_{\text{gua}}$  donor. The electron density donating effect of the dimethylamine substituent leads to relatively stronger donor properties of the  $N_{\text{qu}}$  donor in the Cu(ii) species of **R5**, represented by a positive  $\Delta\Delta E_{\text{CT,qu}}$  value. As a result, a positive  $\Delta\Delta E_{\text{CT,total}}$  value is obtained, indicating a relatively stronger total donation in the Cu(ii) species compared to **R1**. The electron density donating effect of the methyl substituent in **R6** is weaker than of the dimethylamine substituent in **R5**. Further, the effect of the methyl substituent in the 4-position in **R6** is completely different to the effect of the methyl substituent in the 2-position in **R2**. This result confirms that the steric demand of the alkyl substituent in the 2-position is responsible for the relatively stronger total donation in the Cu(i) species of **R2** and **R3** compared to **R1**. **R7** exhibits the opposite results compared to **R5** and **R6** due to the electron density withdrawing effect of the methyl ester substituent.

In comparison, the electronic influence of the substituents in the 4-position affects the relative donor properties of the  $N_{\text{gua}}$  and  $N_{\text{qu}}$  donor in **R5**–**R7** more weakly than the steric demand of the substituents in the 2-position in **R2** and **R3**. Nevertheless, the weaker influence on the relative donor properties of the  $N_{\text{qu}}$  donor in **R5**–**R7** has a more substantial effect on the relative theoretical stabilization of the Cu(i) and Cu(ii) species than the stronger influence on the relative donor properties of the  $N_{\text{gua}}$  donor in **R2** and **R3**. Therefore, the relative theoretical stabilization of the Cu(i) and Cu(ii) species of





the redox couples is more affected by the donor properties of  $N_{\text{qu}}$  donor than by that of the  $N_{\text{gua}}$  donor, resulting in the two different linear correlations (Fig. 6).

The results of **R4** do not fit to any of the two correlations because of the interactions between the copper center and the methyl ester substituent, especially the 4 + 2 coordination motif in **C8**. The  $\Delta\Delta E_{\text{CT},\text{total}}$  value that includes the O donors is significantly higher compared to all other redox couples, indicating the highest relative total donation in a Cu(II) species. However, the smallest  $\Delta\Delta E_{\text{GS},\text{DFT}}$  value is obtained for **R4**, indicating a similar relative theoretical stabilization compared to **R1**. The neglect of the O donors results in a  $\Delta\Delta E_{\text{CT},\text{total}}$  value that fits better to the  $\Delta\Delta E_{\text{GS},\text{DFT}}$  value (Fig. 6,  $\Delta\Delta E_{\text{CT},\text{total}}$  value without the O donors in black and with O donors in red). Therefore, the charge-transfer energies of the O donors are assumed to be overestimated, especially of the  $O_{\text{acyl}}$  donor in **C8**.

### Electrochemical properties

The redox potentials  $E_{1/2}$  were determined by cyclic voltammetry in MeCN starting from the Cu(I) complexes and were referenced against the  $\text{Fc}/\text{Fc}^+$  redox couple as an internal standard (exem-

plarily shown for **R6** in Fig. 7, for **R7** see Fig. S7 in the ESI†). The cyclic voltammograms indicate a reversible one-electron redox process caused by the similar structures of the related Cu (I) and Cu(II) complexes and the absence of any side reactions. The results of the novel redox couples **R6** and **R7** are compared with the redox couples **R1–R5** from the previous study (Table 4).<sup>23</sup> In the previous study, we already discussed a correlation between the redox potential  $E_{1/2}$  and the donor properties of the ligands and the results of **R6** and **R7** further support this correlation. The plot of the redox potential  $E_{1/2}$  representing the relative electrochemical stabilization against the referenced total charge-transfer energy difference  $\Delta\Delta E_{\text{CT},\text{total}}$  shows that a relatively stronger total donation in the Cu(I) species of a redox couple compared to **R1** leads to an increase in the relative electrochemical stabilization of the Cu(I) species and *vice versa* (Fig. 8). Hence, the relative electrochemical stabilization can be estimated based on the relative total donor properties of the ligands. Further, two linear correlations depending on the substituent position are visible, which is analogous to the correlation between the relative theoretical stabilization and the relative total donor properties (Fig. 6 and 8). As noted earlier, this is caused by the different ways the substituents affect the  $N_{\text{gua}}$  and  $N_{\text{qu}}$  donor. This accordance between the experimental electrochemical relative stabilization and the calculated relative stabilization verifies the results of the DFT calculations.

Since the relative theoretical stabilization and the relative electrochemical stabilization correlate in the same way with the relative donor properties, the direct correlation between both expressions for the relative stabilization is of interest. The plot of the redox potential  $E_{1/2}$  against the referenced ground state energy difference  $\Delta\Delta E_{\text{GS},\text{DFT}}$  shows a good correlation between the relative electrochemical stabilization and the relative theoretical stabilization for all redox couples except for **R4** (Fig. 9). A relatively stronger theoretical stabilization of the Cu (I) species of a redox couple compared to **R1** indicated by a positive  $\Delta\Delta E_{\text{GS},\text{DFT}}$  value results in a relatively stronger electrochemical stabilization of the Cu(I) species a redox couple and, therefore, in a higher redox potential compared to **R1**. Additionally, the correlation of the redox potential  $E_{1/2}$  and the referenced ground state energy difference  $\Delta\Delta E_{\text{GS},\text{DFT}}$  depends on the position of the substituent leading to two linear corre-

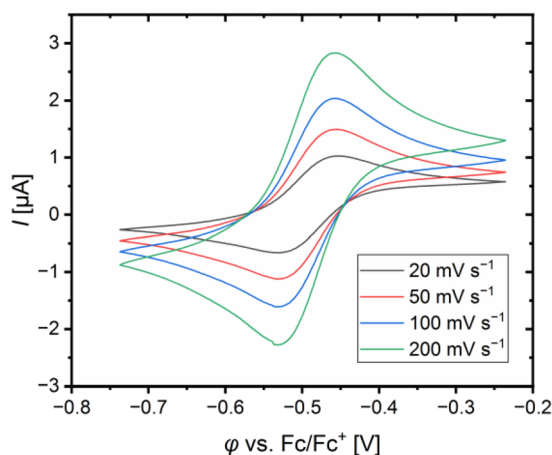
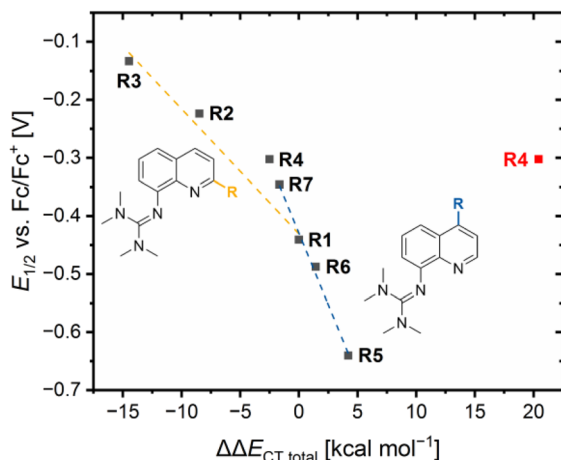


Fig. 7 Cyclic voltammogram of  $[\text{Cu}(\text{TMG4Mequ})_2]^{+2+}$  (**R6**) starting from  $[\text{Cu}(\text{TMG4Mequ})_2]\text{PF}_6$  ( $c = 1 \text{ mM}$ ) in MeCN with  $[\text{NBu}_4][\text{PF}_6]$  ( $c = 100 \text{ mM}$ ).

Table 4 Experimental redox potentials  $E_{1/2}$  vs.  $\text{Fc}/\text{Fc}^+$  and vs. **R1**, referenced charge-transfer energy differences  $\Delta\Delta E_{\text{CT},\text{total}}$ , referenced ground state energy differences  $\Delta\Delta E_{\text{GS},\text{DFT/CCSD(T)}}$  and theoretical redox potentials  $E_{\text{theo,DFT/CCSD(T)}}$  vs. **R1** of **R1–R7** (experimental redox potentials  $E_{1/2}$  vs.  $\text{Fc}/\text{Fc}^+$  of **R1–R5** from previous study;<sup>21</sup> DFT: TPSSh, def2-TZVP, GD3BJ, PCM (MeCN), NBO6.0; DLPNO-CCSD(T): def2-TZVP, def2-TZVP/C, C-PCM (MeCN))

	Exp.		DFT			DLPNO-CCSD(T)	
	$E_{1/2}$ vs. $\text{Fc}/\text{Fc}^+$ [V]	$E_{1/2}$ vs. <b>R1</b> [V]	$\Delta\Delta E_{\text{CT},\text{total}}$ [kcal mol <sup>-1</sup> ]	$\Delta\Delta E_{\text{GS},\text{DFT}}$ [kJ mol <sup>-1</sup> ]	$E_{\text{theo,DFT}}$ vs. <b>R1</b> [V]	$\Delta\Delta E_{\text{GS},\text{CCSD(T)}}$ [kJ mol <sup>-1</sup> ]	$E_{\text{theo,CCSD(T)}}$ vs. <b>R1</b> [V]
$[\text{Cu}(\text{TMGqu})_2]^{+2+}$ ( <b>R1</b> )	−0.441	0.000	0.0	0.000	0.000	0.000	0.000
$[\text{Cu}(\text{TMG2Mequ})_2]^{+2+}$ ( <b>R2</b> )	−0.224	0.217	−8.5	12.664	0.131	15.159	0.157
$[\text{Cu}(\text{TMG2}^c\text{Hexqu})_2]^{+2+}$ ( <b>R3</b> )	−0.134	0.307	−14.5	23.338	0.242	34.165	0.354
$[\text{Cu}(\text{TMG2Meequ})_2]^{+2+}$ ( <b>R4</b> )	−0.302	0.138	−2.5 (20.4)	−1.235	−0.013	13.799	0.143
$[\text{Cu}(\text{TMG4NMe}_2\text{qu})_2]^{+2+}$ ( <b>R5</b> )	−0.640	−0.199	4.2	−28.446	−0.295	−14.539	−0.151
$[\text{Cu}(\text{TMG4Mequ})_2]^{+2+}$ ( <b>R6</b> )	−0.488	−0.047	1.4	−6.423	−0.067	−4.075	−0.042
$[\text{Cu}(\text{TMG4Meequ})_2]^{+2+}$ ( <b>R7</b> )	−0.346	0.095	−1.7	14.852	0.154	6.291	0.065





**Fig. 8** Plot of the redox potentials  $E_{1/2}$  against the referenced charge-transfer energy differences  $\Delta\Delta E_{CT,total}$  of **R1**–**R7** (yellow correlation considers **R1** and in 2-position alkyl-substituted redox couples, blue correlation considers **R1** and in 4-position substituted redox couples, data point of **R4** that also considers the O donors is marked in red).

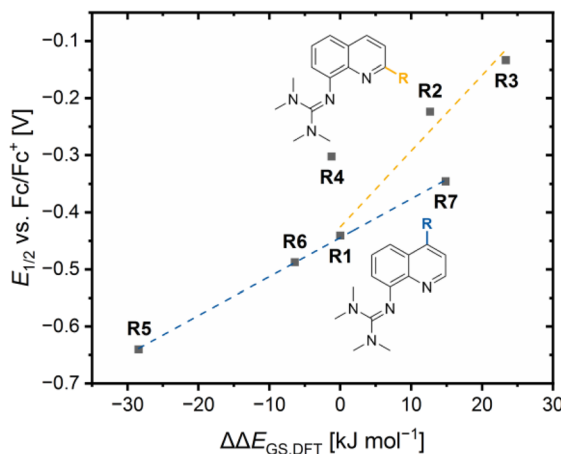


**Fig. 9** Plot of the redox potentials  $E_{1/2}$  vs.  $Fc/Fc^+$  against the referenced ground state energy differences  $\Delta\Delta E_{GS,DFT}$  of **R1**–**R7** (yellow correlation considers **R1** and in 2-position alkyl-substituted redox couples, blue correlation considers **R1** and in 4-position substituted redox couples).

lations. The reason is again the different ways the substituents affect the relative donor properties of the  $N_{gua}$  and  $N_{qu}$  donor in dependency of the substituent position (see discussion of the NBO results of the complexes). As before, **R4** does not fit into the correlation, since the slightly increased relative theoretical stabilization of the  $Cu(II)$  species contradicts the significantly increased relative electrochemical stabilization of the  $Cu(I)$  species compared to **R1**. The reason for the misfit could again be the extraordinary 4 + 2 coordination motif in **C8** compared to the other complexes.

Due to the correlation between the experimental redox potential  $E_{1/2}$  and the referenced ground state energy differences  $\Delta\Delta E_{GS}$ , the calculation of theoretical redox potentials  $E_{theo}$  was performed. The absolute redox potential depends on

the Gibbs free energy difference  $\Delta G$  between the  $Cu(I)$  and  $Cu(II)$  species of a redox couple (eqn (5)).

$$E_{abs} = \frac{\Delta G}{n \cdot F} \quad (5)$$

In a previous study, we calculated the Gibbs free energy difference  $\Delta G$  using a Born–Haber cycle.<sup>41</sup> Here, the ground state energy difference  $\Delta E_{GS,DFT}$  was used instead of the Gibbs free energy difference  $\Delta G$  as a simplification (eqn (6)).

$$E_{abs,theo}(RX) = \frac{\Delta E_{GS}(RX)}{F} \quad (6)$$

To obtain a redox potential  $E_{theo}$  relative to the redox potential of **R1**, the referenced ground state energy differences  $\Delta\Delta E_{GS,DFT}$  was used (eqn (7) and Table 4).

$$E_{theo}(RX)_{vs.R1} = \frac{\Delta\Delta E_{GS}(RX)}{F} \quad (7)$$

Next to theoretical redox potential  $E_{theo,DFT}$  based on the referenced ground state energy differences  $\Delta\Delta E_{GS,DFT}$  determined by DFT calculations, theoretical redox potentials  $E_{theo,CCSD(T)}$  based on the referenced ground state energy differences  $\Delta\Delta E_{GS,CCSD(T)}$  determined by domain-based local pair natural orbital coupled cluster with singles, doubles and perturbative triples excitations (DLPNO-CCSD(T)) calculations were calculated (Table 4,  $E_{GS,CCSD(T)}$  and  $\Delta E_{GS,CCSD(T)}$  values provided in Table S9 in the ESI†). The DLPNO-CCSD(T) calculations were conducted applying the basis set def2-TZVP, the auxiliary basis set def2-TZVP/C and the conductor-like polarizable continuum model (C-PCM) as solvent model for MeCN (further information in the ESI†). The plot of the theoretical redox potentials  $E_{theo,DFT/CCSD(T)}$  against the experimental redox potentials  $E_{1/2}$  indicates the accuracy of the results (Fig. 10). The DFT based theoretical redox potentials  $E_{theo,DFT}$  of **R2**–**R6** are lower than the experimental redox potentials  $E_{1/2}$  whereas for **R7** the opposite case is present. The mean devi-

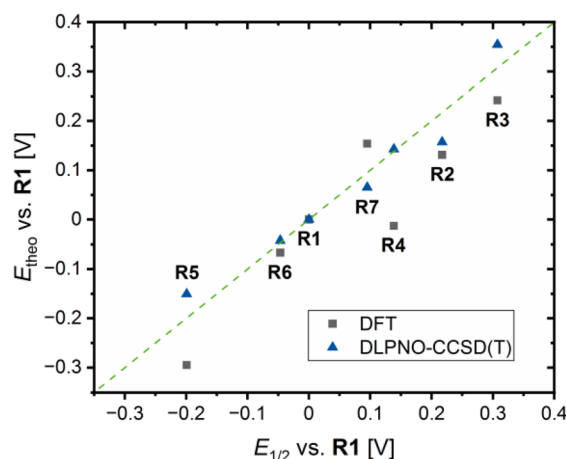


**Fig. 10** Plot of the theoretical redox potentials  $E_{theo,DFT/CCSD(T)}$  vs. **R1** against the experimental redox potentials  $E_{1/2}$  vs. **R1** of **R1**–**R7** (green line represents perfect accordance between both values).



ation between experimental and computed values of **R2–R7** is 0.079 V. However, the shift of the redox potential compared to **R1** is estimated correctly by the DFT based theoretical redox potentials  $E_{\text{theo,DFT}}$  for **R2**, **R3** and **R5–R7**. For **R4**, the influence of the methyl ester substituent is not as well predicted as the influence of the other substituents, which could be caused by the coordinative interactions between the copper center and the methyl ester substituent. Compared to the DFT based theoretical redox potentials  $E_{\text{theo,DFT}}$ , the DLPNO-CCSD(T) based theoretical redox potentials  $E_{\text{theo,CCSD(T)}}$  of **R2–R7** fit even better to the experimental redox potentials  $E_{1/2}$  resulting in a smaller mean deviation of 0.033 V. In particular, the influence of the methyl ester substituent in **R4** is much better predicted by the DLPNO-CCSD(T) calculations than by the DFT calculations. In general, this method proved to be suitable for the estimation of redox potentials with a good accuracy despite small effort. Usually, the determination of theoretical redox potentials of larger molecules like copper complex redox couples is complicated since a redox potential is defined by the small energy difference between the comparable large total energy values of the reduced and oxidized species of a redox couple. These total energy values contain each an energy value defined by the structure and a solvation energy contribution. If a redox process causes significant changes in the structure and the solvent sphere, the exact calculation of the difference in the total energy values is more difficult than for small changes in the structure and the solvent sphere.<sup>42</sup> Usually, the Cu(I) and Cu(II) species of a redox couple possess significantly different structures because Cu(I) and Cu(II) each favor different coordination numbers and geometries.<sup>14</sup> Therefore, the accurate determination of theoretical redox potentials is still challenging.<sup>42</sup> The reason for the relatively good accuracy of the DFT based theoretical redox potentials  $E_{\text{theo,DFT}}$  of **R2**, **R3** and **R5–R7** is presumably the high structural similarity between the related Cu(I) and Cu(II) species. In contrast, the low accuracy of the DFT based theoretical redox potentials  $E_{\text{theo,DFT}}$  of **R4** is probably caused by the larger structural differences between the Cu(I) and Cu(II) species or by an overestimated stabilizing effect of the methyl ester substituent in the Cu(II) species. The high accuracy of the DLPNO-CCSD(T) based theoretical redox potentials  $E_{\text{theo,CCSD(T)}}$  of **R4** despite the same large structural differences between the Cu(I) and Cu(II) species indicates that the DFT calculations overestimate the stabilizing influence of the interactions between Cu(II) center and the methyl ester substituent.

### Electron transfer studies

The electron transfer properties of **R6** and **R7** were analyzed like these of **R1–R5** in the previous study by determination of the electron self-exchange rate  $k_{11}$  using the Marcus cross relation (eqn (8)–(11)). The Marcus cross relation is based on the Marcus theory describing the mechanism of the outer-sphere electron transfer between two metal complexes.<sup>43</sup> The electron self-exchange rate  $k_{11}$  is the reaction rate of the electron transfer reaction between the reduced and the oxidized species of the same redox couple. An electron is transferred from the reduced to the oxidized species resulting in the same

species as before the electron transfer. In case of the copper redox couples the electron is transferred from the Cu(I) species to the Cu(II) species (Scheme 3, top). Since the electron self-exchange rate depends on the temperature, the solvent and the activity coefficient of the reactants, a direct comparison of electron self-exchange rates  $k_{11}$  of different redox couples is only applicable if they were determined under same conditions. For the determination of the electron self-exchange rate  $k_{11}$  via the Marcus cross relation, the reaction rate  $k_{12}$  of a cross reaction between one species of the investigated redox couple and a counter complex has to be determined (Scheme 3, bottom). The counter complex itself is the reduced or oxidized species of the counter complex redox couple, whose electron self-exchange rate  $k_{22}$  must be known (Scheme 3, middle). During the cross reaction, the counter complex oxidizes or reduces the reduced or oxidized species of the analyzed redox couple. In the ideal case, it would make no difference whether the oxidation or the reduction is analyzed to determine the electron self-exchange rate  $k_{11}$ . Nevertheless, the direct comparison is only possible if the same counter complex is used since only a small measurement uncertainty in the electron self-exchange rate  $k_{22}$  of the counter complex redox couple can result in a large error. In accordance with the previous study, the counter complex  $[\text{Co}(\text{bpy})_3]^{3+}$  of the counter complex redox couple  $[\text{Co}(\text{bpy})_3]^{2+/3+}$  was used (Scheme 3, middle).<sup>23</sup> Due to the redox potential of  $[\text{Co}(\text{bpy})_3]^{2+/3+}$ , the Cu(I) species of **R6** and **R7** are oxidized by  $[\text{Co}(\text{bpy})_3]^{3+}$  (Scheme 3, bottom). The electron self-exchange rate  $k_{22}$  of  $[\text{Co}(\text{bpy})_3]^{2+/3+}$  in MeCN at 298 K is reported in the literature.<sup>44</sup>

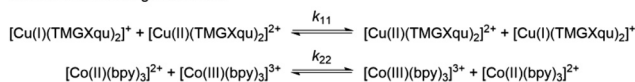
$$k_{11} = \frac{k_{12}^2}{k_{22} \cdot K_{12} \cdot f_{12} \cdot W_{12}^2} \quad (8)$$

$$K_{12} = \exp\left(\frac{\Delta E_{1/2} \cdot n \cdot F}{R \cdot T}\right) \quad (9)$$

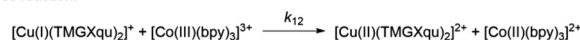
$$f_{12} = \exp\left(\frac{\left(\ln K_{12} + \frac{w_{12} - w_{21}}{R \cdot T}\right)^2}{4 \cdot \left(\ln\left(\frac{k_{22} \cdot k_{22}}{Z^2}\right) + \frac{w_{11} + w_{22}}{R \cdot T}\right)}\right) \quad (10)$$

$$W_{12} = \exp\left(\frac{w_{11} + w_{22} - w_{12} - w_{21}}{2 \cdot R \cdot T}\right) \quad (11)$$

electron self-exchange reactions:



cross reaction:



**Scheme 3** Electron self-exchange reactions of a copper guanidine quinoline redox couple (top) and the counter complex redox couple  $[\text{Co}(\text{bpy})_3]^{2+/3+}$  (middle) and the cross reaction between the Cu(I) species of a copper guanidine quinoline redox couples and the counter complex  $[\text{Co}(\text{bpy})_3]^{3+}$  (bottom) (TMGXqu represents the different guanidine quinoline ligands).



The electron self-exchange rate  $k_{11}$  is calculated with the experimentally determined reaction rate  $k_{12}$  and equilibrium constant  $K_{12}$  (eqn (9)) of the cross reaction, the electron self-exchange rate  $k_{22}$  of the counter complex redox couple, the term  $f_{12}$  (eqn (10)) and the work term  $W_{12}$  (eqn (11)).

Since the cross reaction is a redox reaction, the equilibrium constant  $K_{12}$  is defined by the redox potential difference  $\Delta E_{1/2}$  of the copper complex redox couple and the counter complex redox couple (eqn (9) and Table 5).

The reaction rates  $k_{12}$  of the cross reactions of the Cu(I) complexes **C11** and **C13** with the counter complex  $[\text{Co}(\text{bpy})_3]^{3+}$  were determined in MeCN at 298 K using stopped-flow UV/Vis spectroscopy. During the cross reaction UV/Vis spectra were recorded and the time-dependent changes examined (exemplarily shown for **C13** in Fig. 11, left). The cross reactions were performed with an excess of  $[\text{Co}(\text{bpy})_3]^{3+}$  resulting in a nearly constant concentration of  $[\text{Co}(\text{bpy})_3]^{3+}$  throughout the reaction. Therefore, the cross reaction is pseudo-first order which enables the determination of the reaction rate  $k_{\text{obs}}$  by a first order decay fit of the absorption at the absorption maxima of the Cu(I) complex against the reaction time (exemplarily shown for **C13** in Fig. 11, middle). The reaction rate  $k_{\text{obs}}$  was determined for five different concentrations of  $[\text{Co}(\text{bpy})_3]^{3+}$ . By a linear fit of the reaction rate  $k_{\text{obs}}$  against the concentration of

$[\text{Co}(\text{bpy})_3]^{3+}$ , the reaction rate  $k_{12}$  is obtained (exemplarily shown for **C13** in Fig. 11, right; for **C11** see Fig. S10 in the ESI† Table 5). The influence of the ionic strength on the activity coefficients of the reactants is neglected.

Following the Marcus cross relation, the electron self-exchange rates  $k_{11}$  of **R6** and **R7** were calculated and compared with those of **R1–R5** from the previous study (eqn (8) and Table 5).<sup>23</sup> For **R6**, a similar electron self-exchange rate  $k_{11}$  compared to **R1** is obtained. Therefore, the methyl substituent in the 4-position and its weak electronic effect have no significant influence on the electron transfer. Further, **R6** and **R1** possess identical  $\Delta\tau_4$  and  $\emptyset\tau_4$  parameter because the methyl substituent in the 4-position does not exhibit any steric demand. Hence, from the structural point of view, they are similar entatic state models and, therefore, similar electron self-exchange rates are expectable. Compared to **R6**, the methyl substituent in the 2-position of **R2** exhibits a steric demand resulting in more similar structures of the Cu(I) and Cu(II) species indicated by a smaller  $\Delta\tau_4$  parameter and, thus, in a higher electron self-exchange rate  $k_{11}$  compared to **R1**. This results shows that the steric demand of the methyl substituent in the 2-position of **R2** is crucial for the accelerated electron transfer and the enhanced ability as entatic state model. For **R7**, an electron self-exchange rate  $k_{11}$  half as large but in the

**Table 5** Redox potential differences  $\Delta E_{1/2}$  between **R1–R7** and the counter complex redox couple  $[\text{Co}(\text{bpy})_3]^{2+/3+}$ , equilibrium constants  $K_{12}$  and reaction rates  $k_{12}$  of the cross reactions between the Cu(I) species of **R1–R7** and the counter complex  $[\text{Co}(\text{bpy})_3]^{3+}$  and electron self-exchange rates  $k_{11}$  and calculated  $\emptyset\tau_4$  and  $\Delta\tau_4$  parameters of **R1–R7** (values of **R1–R5** from previous study<sup>21</sup>)

	$\Delta E_{1/2}$ [V]	$K_{12}$ [ ]	$k_{12}$ [ $\text{M}^{-1} \text{s}^{-1}$ ]	$k_{11}$ [ $\text{M}^{-1} \text{s}^{-1}$ ]	$\Delta\tau_{4,\text{DFT}}$ [ ]	$\emptyset\tau_{4,\text{DFT}}$ [ ]
$[\text{Cu}(\text{TMGqu})_2]^{+/2+}$ ( <b>R1</b> )	−0.385	$3.19 \times 10^6$	$(2.31 \pm 0.07) \times 10^4$	$(2.81 \pm 0.18) \times 10^2$	0.20	0.53
$[\text{Cu}(\text{TMG2Mequ})_2]^{+/2+}$ ( <b>R2</b> )	−0.168	$6.81 \times 10^2$	$(1.63 \pm 0.16) \times 10^3$	$(2.19 \pm 0.44) \times 10^3$	0.13	0.59
$[\text{Cu}(\text{TMG2}^t\text{Hexqu})_2]^{+/2+}$ ( <b>R3</b> )	−0.078	$2.04 \times 10^1$	$(2.25 \pm 0.14) \times 10^2$	$(1.15 \pm 0.15) \times 10^3$	0.07	0.68
$[\text{Cu}(\text{TMG2Meequ})_2]^{+/2+}$ ( <b>R4</b> )	−0.246	$1.46 \times 10^4$	$(6.67 \pm 0.30) \times 10^3$	$(2.33 \pm 0.22) \times 10^3$	0.00 <sup>a</sup>	0.61 <sup>a</sup>
$[\text{Cu}(\text{TMG4NMe}_2\text{qu})_2]^{+/2+}$ ( <b>R5</b> )	−0.584	$7.45 \times 10^9$	$(4.74 \pm 0.27) \times 10^5$	$(3.38 \pm 0.44) \times 10^2$	0.20	0.54
$[\text{Cu}(\text{TMG4Mequ})_2]^{+/2+}$ ( <b>R6</b> )	−0.431	$2.52 \times 10^7$	$(4.90 \pm 0.19) \times 10^4$	$(2.38 \pm 0.20) \times 10^2$	0.20	0.53
$[\text{Cu}(\text{TMG4Meequ})_2]^{+/2+}$ ( <b>R7</b> )	−0.290	$9.24 \times 10^4$	$(3.88 \pm 0.16) \times 10^3$	$(1.48 \pm 0.13) \times 10^2$	0.19	0.53

<sup>a</sup> The comparability of this value is limited due to the 4 + 2 coordination motif.

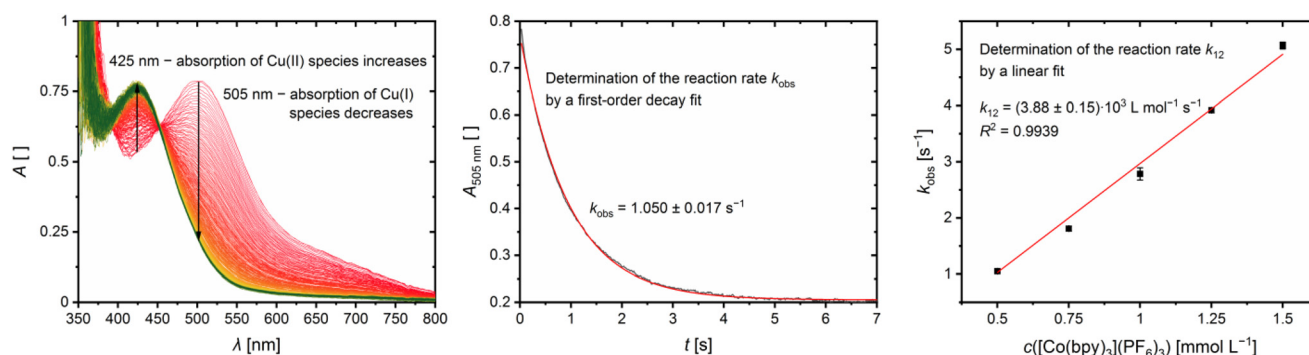


**Fig. 11** Results of the cross reaction of  $[\text{Cu}(\text{TMG4Meequ})_2]^+$  (**C13**) with  $[\text{Co}(\text{bpy})_3]^{3+}$ : time-dependent change of the UV/Vis spectra (left) and time-trace of the Cu(I) absorption band at 505 nm (middle; black: measurement, red: fit) during the cross reaction with an excess of  $[\text{Co}(\text{bpy})_3]^{3+}$  (1 : 5) in MeCN at 298 K and plot of the reaction rate  $k_{\text{obs}}$  against the concentration of  $[\text{Co}(\text{bpy})_3]^{3+}$  (right; black: measurement, red: fit; some error bars are too small to be visualized properly).





same order of magnitude as for **R1** is obtained. Therefore, the methyl ester substituent in the 4-position and its electronic effect slightly decelerates the electron transfer. In our previous study, we found that the methyl ester substituent in the 2-position of **R4** induces a significant increase in the electron self-exchange rate  $k_{11}$ . We made different hypotheses to explain this influence of the methyl ester substituent in the 2-position on the electron transfer.<sup>23</sup> The electron self-exchange rate of **R7** provides new insights into the role of the methyl ester substituent in **R4** regarding the fast electron transfer. The suggested hypothesis that the methyl ester substituent in **R4** could act as an electron bridge for the outer-sphere electron transfer resulting in a shortened jump length of the electron through space can be rejected. If this hypothesis would be the reason for the fast electron transfer of **R4**, a faster electron transfer should also be visible for **R7** because substituents in the 2- and 4-position exhibit similar electronic effects on the aromatic system. Hence, the extraordinary coordinative behavior of the ligand is the reason for the fast electron transfer and the enhanced entatic state whereby two different explanations are possible. First, the additional coordinative interactions between the methyl ester substituent and the copper center could be energetically unfavorable for the copper center. In the Cu(I) species of **R4**, the additionally weak interactions between the methyl ester substituent and the Cu(I) center could be energetically unfavorable since Cu(I) prefers to be four-coordinate in a tetrahedral geometry. In the Cu(II) species of **R4**, the 4 + 2 coordination motif with the two non-axially positioned elongated Cu–O<sub>acyl</sub> bonds could be energetically unfavorable. These energetically unfavored interactions in the Cu(I) and Cu(II) species of **R4** could be comparable to the energetically unfavorable stronger distortion in **R2** and **R3** and, therefore, the reason for the accelerated electron transfer compared to **R1**. Second, the methyl ester substituent could insulate the solvent sphere from the charge of the copper center by its weak donor properties. Hence, the reorganization of the solvent molecules during the electron transfer is reduced resulting in a lower solvent reorganization energy.

To further correlate the determined electron self-exchange rates, the internal, solvent and total reorganization energies  $\lambda_{11,I}$ ,  $\lambda_{11,S}$  and  $\lambda_{11,T}$  of **R6** and **R7** were calculated analogously to **R1–R5** from the previous study (Table 6, necessary energy values provided in Table S10 in the ESI†).<sup>23</sup> Previously, we observed that the internal reorganization energies  $\lambda_{11,I}$  corre-

late with the structural similarity between the related Cu(I) and Cu(II) species of the redox couples and, therefore, with the RMSD values. For all previous redox couples except for **R4**, a linear correlation was found.<sup>23</sup> The results of **R6** and **R7** fit into this linear correlation (Fig. 12). The internal and solvent reorganization energies  $\lambda_{11,I}$  and  $\lambda_{11,S}$  of **R6** are similar to those of **R1** and not decreased like those of **R2**. Hence, also the total reorganization energies  $\lambda_{11,T}$  of **R1** and **R6** are similar which is in accordance with the similar electron self-exchange rates. This underlines again the negligible influence of the methyl substituent in the 4-position on **R6** and the importance of the methyl substituent in the 2-position for the enhanced electron transfer properties of **R2** indicated by the faster electron self-exchange rate  $k_{11}$  and lower total reorganization energy  $\lambda_{11,T}$  compared to **R1**. The internal reorganization energy  $\lambda_{11,I}$  of **R7** is similar to those of **R1** and **R6** because the methyl ester substituent in the 4-position does not affect the structural similarity between the Cu(I) and Cu(II) complex significantly. Therefore, the methyl ester substituent in the 4-position exerts no significant influence on the internal reorganization energy  $\lambda_{11,I}$  of **R7** compared to the methyl ester substituent in the 2-position in **R4**. Further, the position of the methyl ester substituent affects the influence on the solvent reorganization energy  $\lambda_{11,S}$ . Whereas the methyl ester substituent in the 2-position reduces the solvent reorganization energy  $\lambda_{11,S}$  of **R4** significantly compared to **R1**, the influence of the methyl ester substituent in the 4-position on the solvent reorganization energy  $\lambda_{11,S}$  of **R7** is not that strong. This result underlines that the weak coordinative interactions between the methyl ester substituent and the copper center in **R4** result in an insulation of the solvent sphere from the changing charge of the copper center during the electron transfer. Nevertheless, also the solvent reorganization energy  $\lambda_{11,S}$  of **R7** is decreased compared to **R1** without any further coordinative interactions. The reason could be that the extended  $\pi$  system of the ligand in **R7**, caused by the methyl ester substituent, dampens the impact of the changing charge on the solvent sphere stronger than the smaller  $\pi$  system of the ligand in **R1**. In sum, **R7** exhibits a lower total reorganization energy  $\lambda_{11,T}$  than **R4** with is in contrast to the higher electron self-exchange rate of **R4** compared to **R7**. A reason could be that the internal and solvent reorganization energies do not contribute in the same way to the velocity of the electron transfer. Further, this emphasizes that although the calculated reorganization energies give

**Table 6** Calculated internal, solvent and total reorganization energies  $\lambda_{11,I}$ ,  $\lambda_{11,S}$  and  $\lambda_{11,T}$  and calculated RMSD values of **R1–R7** (values of **R1–R5** from previous study<sup>21</sup>)

	$\lambda_{11,I}$ [kJ mol <sup>-1</sup> ]	$\lambda_{11,S}$ [kJ mol <sup>-1</sup> ]	$\lambda_{11,T}$ [kJ mol <sup>-1</sup> ]	RMSD <sub>DFT</sub> [Å]
[Cu(TMGqu) <sub>2</sub> ] <sup>+2+</sup> ( <b>R1</b> )	66.6	135.2	201.8	0.283
[Cu(TMG2Mequ) <sub>2</sub> ] <sup>+2+</sup> ( <b>R2</b> )	55.2	128.6	183.8	0.191
[Cu(TMG2 <sup>c</sup> Hexqu) <sub>2</sub> ] <sup>+2+</sup> ( <b>R3</b> )	52.7	110.7	163.3	0.147
[Cu(TMG2Meequ) <sub>2</sub> ] <sup>+2+</sup> ( <b>R4</b> )	81.6	123.5	205.1	2.289
[Cu(TMG4NMe <sub>2</sub> qu) <sub>2</sub> ] <sup>+2+</sup> ( <b>R5</b> )	77.4	128.2	205.6	0.446
[Cu(TMG4Mequ) <sub>2</sub> ] <sup>+2+</sup> ( <b>R6</b> )	68.5	132.9	201.4	0.282
[Cu(TMG4Meequ) <sub>2</sub> ] <sup>+2+</sup> ( <b>R7</b> )	65.1	129.2	194.2	0.250



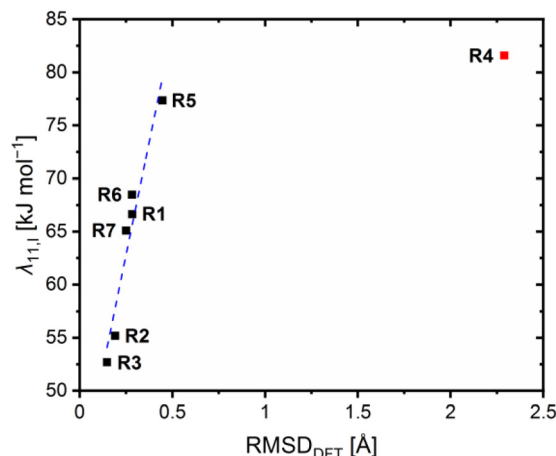


**Fig. 12** Plot of the internal reorganization energies  $\lambda_{11,1}$  against the calculated RMSD values of R1–R7 (blue correlation considers R1–R3, R5–R7, data point of R4 is marked in red due to the misfit to the linear correlation).

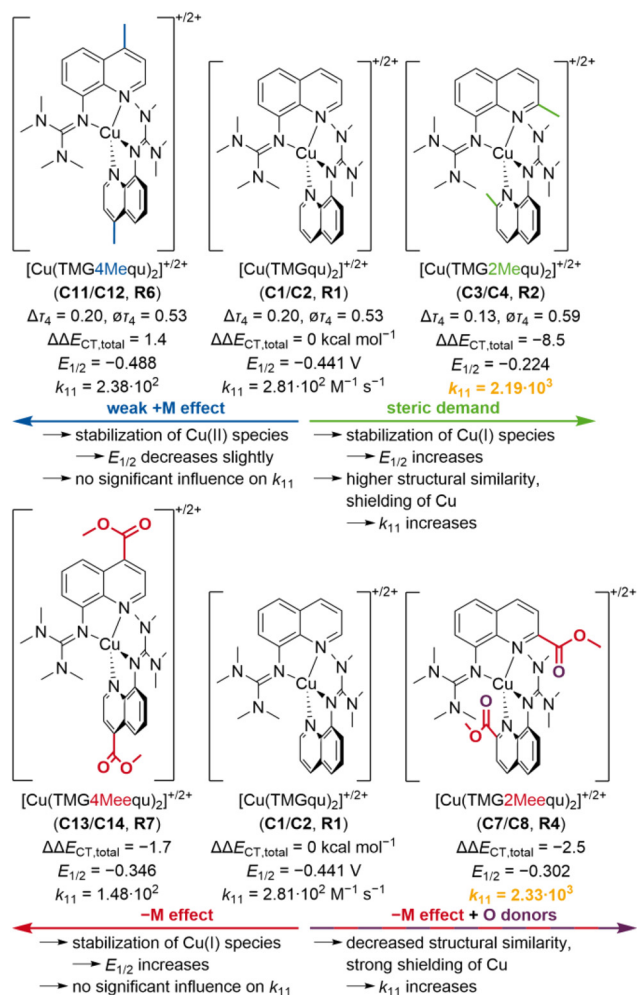


**Fig. 13** Summary of the substituent influences on the properties of the copper complex redox couples R2, R4, R6 and R7 compared to R1 (substituents and initial effects are marked in the same color; two highest electron self-exchange rates are marked in orange; units are only given for R1; redox potentials  $E_{1/2}$  vs. Fc/Fc<sup>+</sup>;  $\Delta E_{CT}$  and  $\phi_{CT}$  parameters, redox potentials  $E_{1/2}$  and electron self-exchange rates  $k_{11}$  of R1, R2 and R4 from previous study<sup>21</sup>).

important insights into the electron transfer properties, their influence should not be overestimated. They are based on theoretically calculated energy values like the theoretical redox potentials  $E_{theo,DFT}$ . In the case of the theoretical redox potentials, the good accuracy enables the estimation of the redox potential but not the exact determination. Hence, this circumstance also applies to the reorganization energies.

## Conclusions

In this study, two novel guanidine quinoline ligands with a methyl or methyl ester substituent in the 4-position were synthesized to analyze the importance of the position on the substituent influence compared to the ligands with a methyl or methyl ester substituent in the 2-position. The related novel Cu(I) and Cu(II) complexes C11–C14 were synthesized and structurally investigated by XRD and DFT calculations, indicating that the 2-position is crucial for the significant substituent influence on the structures of C3, C4, C7 and C8 (Fig. 13). In addition, the donor properties of the ligands were examined by NBO calculations, revealing opposite substituent influences on the complex structures and ligand donor properties are reflected in the redox potentials of the copper complex redox couples R2, R4, R6 and R7 and therefore, in the electrochemical stabilization (Fig. 13). In consideration of the redox potentials and DFT results of R1–R7, an easy method for the estimation of the redox potential with a good accuracy was demonstrated. Finally, the determination of the electron self-exchange rates and reorganization energies of R6 and R7 and the comparison with R2 and R4 indicated that also the electron transfer properties depend significantly on the substituent position (as summarized in Fig. 13). Only the substituents in the 2-position, which affect the structure of the complexes, exert a strong and enhancing influence on the electron transfer properties, whereas the pure electronic influence of substituents in the 4-position is negligible. Overall, the results demonstrate the importance of the position on the substituent influence affecting several properties of the copper complexes and give new crucial insights into the targeted design of better entatic state models.

## Data availability

All synthetic details are described in the ESI.† Additional information on the synthesis of the target compounds and original analysis data files are available in the Chemotion repository (for corresponding links see the ESI†).

## Author contributions

J. H. and A. K. synthesized the ligands and complexes. They performed and evaluated the CV, NMR, IR, UV/Vis measurements. Further, they evaluated the MS measurements. J. H.



performed the stopped-flow UV/Vis spectroscopic measurements and fluorescence spectroscopic measurements and determined the electron self-exchange rates. Furthermore, J. H. and A. K. executed and evaluated the DFT calculations. J. H. executed and evaluated the CREST and DLPNO-CCSD(T) calculations. J. H. determined the reorganization energies applying the Nelsen's four-point method. A. H. checked and finalized the crystallographic data. J. H., A. H. and S. H.-P. wrote the manuscript. S. H.-P. supervised the project.

## Conflicts of interest

There are no conflicts to declare.

## Acknowledgements

S. H.-P. acknowledge financial support by the Deutsche Forschungsgemeinschaft (DFG, 413524714). We thank the Regional Computing Center of the University of Cologne (RRZK) for providing computing time on the DFG-funded High Performance Computing (HPC) system CHEOPS as well as support.

## References

- (a) W. Kaim and J. Rall, *Angew. Chem., Int. Ed. Engl.*, 1996, **35**, 43, (*Angew. Chem.*, 1996, **108**, 47); (b) I. A. Koval, P. Gamez, C. Belle, K. Selmecezi and J. Reedijk, *Chem. Soc. Rev.*, 2006, **35**, 814; (c) R. L. Peterson, S. Kim and K. D. Karlin, in *Comprehensive inorganic chemistry II*, ed. J. Reedijk and K. R. Poeppelmeier, Elsevier, Amsterdam, 2013, pp. 149–177; (d) E. I. Solomon, D. E. Heppner, E. M. Johnston, J. W. Ginsbach, J. Cirera, M. Qayyum, M. T. Kieber-Emmons, C. H. Kjaergaard, R. G. Hadt and L. Tian, *Chem. Rev.*, 2014, **114**, 3659.
- J. Liu, S. Chakraborty, P. Hosseinzadeh, Y. Yu, S. Tian, I. Petrik, A. Bhagi and Y. Lu, *Chem. Rev.*, 2014, **114**, 4366.
- (a) S. Dahlin, B. Reinhammar and M. T. Wilson, *Biochem. J.*, 1984, **218**, 609; (b) F. A. Armstrong, P. C. Driscoll, H. Allen and O. Hill, *FEBS Lett.*, 1985, **190**, 242; (c) A. Lommen and G. W. Canters, *J. Biol. Chem.*, 1990, **265**, 2768; (d) C. Dennison, *Coord. Chem. Rev.*, 2005, **249**, 3025; (e) K. Sato, T. Kohzuma and C. Dennison, *J. Am. Chem. Soc.*, 2003, **125**, 2101.
- B. L. Vallee and R. J. Williams, *Proc. Natl. Acad. Sci. U. S. A.*, 1968, **59**, 498.
- R. J. Williams, *Eur. J. Biochem.*, 1995, **234**, 363.
- P. Comba, *Coord. Chem. Rev.*, 2000, **200–202**, 217.
- J. Stanek, A. Hoffmann and S. Herres-Pawlis, *Coord. Chem. Rev.*, 2018, **365**, 103.
- W. R. Hagen, *Metallomics*, 2019, **11**, 1768.
- R. Lumry and H. Eyring, *J. Phys. Chem.*, 1954, **58**, 110.
- (a) J. M. Berg, J. L. Tymoczko, G. J. Gatto and L. Stryer, *Biochemistry*, Macmillan International Higher Education, New York, 2019; (b) J. A. Yankeelov and D. E. Koshland, *J. Biol. Chem.*, 1965, **240**, 1593; (c) W. W. Cleland, *Acc. Chem. Res.*, 1975, **8**, 145.
- (a) B. Karlsson, R. Aasa, B. G. Malmström and L. G. Lundberg, *FEBS Lett.*, 1989, **253**, 99; (b) B. G. Malmström, *Biol. Met.*, 1990, **3**, 64; (c) B. G. Malmström, *Eur. J. Biochem.*, 1994, **223**, 711.
- G. Chaka, J. L. Sonnenberg, H. B. Schlegel, M. J. Heeg, G. Jaeger, T. J. Nelson, L. A. Ochrymowycz and D. B. Rorabacher, *J. Am. Chem. Soc.*, 2007, **129**, 5217.
- P. Comba and W. Schiek, *Coord. Chem. Rev.*, 2003, **238–239**, 21.
- E. Falcone and C. Hureau, *Chem. Soc. Rev.*, 2023, **52**, 6595.
- (a) A. Das, C. Hessin, Y. Ren and M. Desage-El Murr, *Chem. Soc. Rev.*, 2020, **49**, 8840; (b) L. Garcia, F. Cisnetti, N. Gillet, R. Guillot, M. Aumont-Nicaise, J.-P. Piquemal, M. Desmadril, F. Lambert and C. Policar, *J. Am. Chem. Soc.*, 2015, **137**, 1141; (c) D. Coquière, A. de La Lande, S. Martí, O. Parisel, T. Prangé and O. Reinaud, *Proc. Natl. Acad. Sci. U. S. A.*, 2009, **106**, 10449; (d) N. Le Poul, M. Campion, G. Izzet, B. Douziech, O. Reinaud and Y. Le Mest, *J. Am. Chem. Soc.*, 2005, **127**, 5280; (e) S. Warzeska and R. Krämer, *Chem. Commun.*, 1996, **52**, 499; (f) Y. Ren, J. Forté, K. Cheaib, N. Vanthuyne, L. Fensterbank, H. Vezin, M. Orio, S. Blanchard and M. Desage-El Murr, *iScience*, 2020, **23**, 100955; (g) P. J. Griffin, B. J. Charette, J. H. Burke, J. Vura-Weis, R. D. Schaller, D. J. Gosztola and L. Olshansky, *J. Am. Chem. Soc.*, 2022, **144**, 12116; (h) J. Vallejo, E. Pardo, M. Viciano-Chumillas, I. Castro, P. Amorós, M. Déniz, C. Ruiz-Pérez, C. Yuste-Vivas, J. Krzystek, M. Julve, F. Lloret and J. Cano, *Chem. Sci.*, 2017, **8**, 3694.
- (a) B. Xie, T. Elder, L. J. Wilson and D. M. Stanbury, *Inorg. Chem.*, 1999, **38**, 12; (b) B. Xie, L. J. Wilson and D. M. Stanbury, *Inorg. Chem.*, 2001, **40**, 3606.
- P. Comba, M. Kerscher and A. Roodt, *Eur. J. Inorg. Chem.*, 2004, **2004**, 4640.
- E. W. Dahl and N. K. Szymczak, *Angew. Chem., Int. Ed.*, 2016, **55**, 3101, (*Angew. Chem.*, 2016, **128**, 3153).
- A. Hoffmann, S. Binder, A. Jesser, R. Haase, U. Flörke, M. Gnida, M. Salomone Stagni, W. Meyer-Klaucke, B. Lebsanft, L. E. Grünig, S. Schneider, M. Hashemi, A. Goos, A. Wetzel, M. Rübhausen and S. Herres-Pawlis, *Angew. Chem., Int. Ed.*, 2014, **53**, 299, (*Angew. Chem.*, 2014, **126**, 305).
- A. Hoffmann, J. Stanek, B. Dicke, L. Peters, B. Grimm-Lebsanft, A. Wetzel, A. Jesser, M. Bauer, M. Gnida, W. Meyer-Klaucke, M. Rübhausen and S. Herres-Pawlis, *Eur. J. Inorg. Chem.*, 2016, **2016**, 4731.
- J. Stanek, N. Sackers, F. Fink, M. Paul, L. Peters, R. Grunzke, A. Hoffmann and S. Herres-Pawlis, *Chem. – Eur. J.*, 2017, **23**, 15738.
- J. Stanek, M. Konrad, J. Mannsperger, A. Hoffmann and S. Herres-Pawlis, *Eur. J. Inorg. Chem.*, 2018, **2018**, 4997.
- J. Heck, F. Metz, S. Buchenau, M. Teubner, B. Grimm-Lebsanft, T. P. Spaniol, A. Hoffmann, M. A. Rübhausen and S. Herres-Pawlis, *Chem. Sci.*, 2022, **13**, 8274.



- 24 (a) O. H. Johnson and C. S. Hamilton, *J. Am. Chem. Soc.*, 1941, **63**, 2864; (b) S. Lutun, E. Guichard, B. Hasiak and D. Couturier, *Synth. Commun.*, 1999, **29**, 175; (c) H. Chen, P. Li, M. Wang and L. Wang, *Eur. J. Org. Chem.*, 2018, **2018**, 2091.
- 25 T. Rösener, A. Hoffmann and S. Herres-Pawlis, *Eur. J. Inorg. Chem.*, 2018, **2018**, 3164.
- 26 (a) W. Kantlehner, E. Haug, W. W. Mergen, P. Speh, T. Maier, J. J. Kapassakalidis, H.-J. Bräuner and H. Hagen, *Liebigs Ann. Chem.*, 1984, **1984**, 108; (b) S. Herres-Pawlis, A. Neuba, O. Seewald, T. Seshadri, H. Egold, U. Flörke and G. Henkel, *Eur. J. Org. Chem.*, 2005, 4879.
- 27 J. Tao, J. P. Perdew, V. N. Staroverov and G. E. Scuseria, *Phys. Rev. Lett.*, 2003, **91**, 146401.
- 28 V. N. Staroverov, G. E. Scuseria, J. Tao and J. P. Perdew, *J. Chem. Phys.*, 2003, **119**, 12129.
- 29 A. Schäfer, C. Huber and R. Ahlrichs, *J. Chem. Phys.*, 1994, **100**, 5829.
- 30 K. Eichkorn, F. Weigend, O. Treutler and R. Ahlrichs, *Theor. Chem. Acc.*, 1997, **97**, 119.
- 31 F. Weigend and R. Ahlrichs, *Phys. Chem. Chem. Phys.*, 2005, **7**, 3297.
- 32 S. Grimme, S. Ehrlich and L. Goerigk, *J. Comput. Chem.*, 2011, **32**, 1456.
- 33 L. Goerigk and S. Grimme, *Phys. Chem. Chem. Phys.*, 2011, **13**, 6670.
- 34 A. Hoffmann, R. Grunzke and S. Herres-Pawlis, *J. Comput. Chem.*, 2014, **35**, 1943.
- 35 A. Hoffmann, M. Rohrmüller, A. Jesser, I. dos Santos Vieira, W. G. Schmidt and S. Herres-Pawlis, *J. Comput. Chem.*, 2014, **35**, 2146.
- 36 (a) A. Jesser, M. Rohrmüller, W. G. Schmidt and S. Herres-Pawlis, *J. Comput. Chem.*, 2014, **35**, 1; (b) M. Rohrmüller, S. Herres-Pawlis, M. Witte and W. G. Schmidt, *J. Comput. Chem.*, 2013, **34**, 1035; (c) M. Rohrmüller, A. Hoffmann, C. Thierfelder, S. Herres-Pawlis and W. G. Schmidt, *J. Comput. Chem.*, 2015, **36**, 1672.
- 37 T. Rösener, O. Bienemann, K. Sigl, N. Schopp, F. Schnitter, U. Flörke, A. Hoffmann, A. Döring, D. Kuckling and S. Herres-Pawlis, *Chem. – Eur. J.*, 2016, **22**, 13550.
- 38 P. Liebhäuser, K. Keisers, A. Hoffmann, T. Schnappinger, I. Sommer, A. Thoma, C. Wilfer, R. Schoch, K. Stührenberg, M. Bauer, M. Dürr, I. Ivanović-Burmazović and S. Herres-Pawlis, *Chem. – Eur. J.*, 2017, **23**, 12171.
- 39 L. Yang, D. R. Powell and R. P. Houser, *Dalton Trans.*, 2007, 955.
- 40 A. Wagner and H.-J. Himmel, *J. Chem. Inf. Model.*, 2017, **57**, 428.
- 41 L. Raßpe-Lange, A. Hoffmann, C. Gertig, J. Heck, K. Leonhard and S. Herres-Pawlis, *J. Comput. Chem.*, 2023, **44**, 319.
- 42 L. Yan, Y. Lu and X. Li, *Phys. Chem. Chem. Phys.*, 2016, **18**, 5529.
- 43 (a) R. A. Marcus, *Pure Appl. Chem.*, 1997, **69**, 13; (b) R. A. Marcus, *Angew. Chem., Int. Ed. Engl.*, 1993, **32**, 1111, (*Angew. Chem.*, 1993, **105**, 1161); (c) R. A. Marcus and N. Sutin, *Biochim. Biophys. Acta, Rev. Bioenerg.*, 1985, **811**, 265.
- 44 B. C. Dunn, L. A. Ochrymowycz and D. B. Rorabacher, *Inorg. Chem.*, 1995, **34**, 1954.

